

K2 rotation periods for low-mass Hyads and a quantitative comparison of the distribution of slow rotators in the Hyades and Praesepe

S. T. DOUGLAS,^{1,*} J. L. CURTIS,^{2,*} M. A. AGÜEROS,² P. A. CARGILE,¹ J. M. BREWER,^{3,2} S. MEIBOM,¹ AND T. JANSEN²

¹*Center for Astrophysics / Harvard & Smithsonian, 60 Garden St, Cambridge, MA 02138, USA*

²*Department of Astronomy, Columbia University, 550 West 120th Street, New York, NY 10027, USA*

³*Department of Astronomy, Yale University, 52 Hillhouse Avenue, New Haven, CT 06511, USA*

ABSTRACT

We analyze *K2* light curves for 132 low-mass ($1 \gtrsim M_* \gtrsim 0.1 M_\odot$) members of the 600–800 Myr-old Hyades cluster and measure rotation periods (P_{rot}) for 116 of these stars. These include 93 stars with no prior P_{rot} measurement; the total number of Hyads with known P_{rot} is now 232. We then combine literature binary data with *Gaia* DR2 photometry and astrometry to select single star sequences in the Hyades and its roughly coeval Praesepe open cluster, and derive a new reddening value of $A_V = 0.035 \pm 0.011$ for Praesepe. Comparing the effective temperature– P_{rot} distributions for the Hyades and Praesepe, we find that solar-type Hyads rotate, on average, 0.4 d slower than their Praesepe counterparts. This P_{rot} difference indicates that the Hyades is slightly older than Praesepe: we apply a new gyrochronology model tuned with Praesepe and the Sun, and find an age difference between the two clusters of 57 Myr. However, this P_{rot} difference decreases and eventually disappears for lower-mass stars. This provides further evidence for stalling in the rotational evolution of these stars, and highlights the need for more detailed analysis of angular-momentum evolution for stars of different masses and ages.

Keywords: open clusters: individual (Hyades, Praesepe) — stars: evolution – stars: late-type – stars: rotation

1. INTRODUCTION

The Hyades and Praesepe open clusters are benchmarks for determining the dependence of stellar rotation on age. The Hyades was one of the first open clusters for which photometric rotation periods (P_{rot}) were measured for low-mass stars ($\lesssim 1 M_\odot$; Radick et al. 1987, 1995). The two clusters are sufficiently nearby such that many photometric P_{rot} across the full FGKM mass range have now been measured for both from ground- and space-based photometric monitoring (e.g., Agüeros et al. 2011; Delorme et al. 2011; Hartman et al. 2011; Douglas et al. 2014, 2016, 2017; Rebull et al. 2017).

Empirical efforts to establish the functional form of the rotation-age relation, sometimes referred to as gyrochronology (Barnes 2003), have commonly assumed that the mass dependence can be separated from the age dependence, such that $P_{rot}(M_*, t) = f(M_*) \times g(t)$. This

was famously proposed by Skumanich (1972), who found that solar-type stars spin down as $P_{rot} \propto t^n$, where the braking index $n \approx 0.5$. Barnes (2003, 2007) accounted for the dependence on mass by adopting photometric color as its observational proxy, then fit coefficients for a simple analytic function from observations of rotators with a range of masses in young nearby clusters. The resulting model implied that lower-mass stars spin down more rapidly than their solar-type counterparts. Later authors (e.g., Mamajek & Hillenbrand 2008; Meibom et al. 2009; Angus et al. 2015) have adjusted the coefficients and braking index, but otherwise have assumed the same functional form as Barnes. However, an examination of the figures in Barnes (2003) shows that this fixed relation between P_{rot} , t , and color is insufficient to describe stellar spin-down for stars with a range of masses.

More recent P_{rot} measurements for G and K dwarfs in open clusters have shown that P_{rot} evolution cannot be described by separating the mass and age dependence. Using the Skumanich relation, Meibom et al. (2011b) tested whether Hyades rotators could be spun up to

Corresponding author: S. T. Douglas
StephanieTDouglas@gmail.com

* NSF Astronomy and Astrophysics Postdoctoral Fellow

match the observed distribution of P_{rot} in M34, which is 220 Myr old. These authors determined that while the distribution of spun-up solar-type Hyads did match that of their younger cousins, spinning up Hyades K dwarfs by the same factor resulted in these stars having faster P_{rot} than those observed in M34. Comparing P_{rot} measured for GK stars in various open clusters from 100 Myr to 1 Gyr leads to a similar conclusion: Skumanich-like spin-down works well for solar-type stars, but K dwarfs spin down more slowly (Meibom et al. 2011b; Cargile et al. 2014; Agüeros et al. 2018).

Furthermore, while re-tuning the coefficients for the Barnes (2007) gyrochronology equation, Angus et al. (2015) could not simultaneously fit Praesepe and the Hyades. When including Praesepe, these authors' fit resulted in a multi-modal distribution for their color singularity term, which controls the downturn toward rapid rotation for bluer/hotter/more massive stars (which have thinner convective envelopes, resulting in relatively weaker magnetic dynamos and braking efficiency). This is additional evidence that the shape of the slow-rotator sequence can vary from cluster to cluster.

A complication in using the Hyades and Praesepe for calibrating gyrochronology is that their absolute and relative ages, usually determined from isochrones, are still debated (see Table 1 for examples of ages derived for the two clusters). Most authors agree that the clusters are either coeval, or that the Hyades is slightly older, and that their ages range from ≈ 600 to ≈ 800 Myr. But the disagreements among these ages do not provide much hope that we can successfully calibrate gyrochronology using isochronal cluster ages. And it creates confusion for gyrochronology studies: some authors separate the two clusters when comparing data to theoretical models (Brown 2014; Matt et al. 2015; Garraffo et al. 2018), while others combine them (Reiners & Mohanty 2012; Angus et al. 2015).

Our goal is to compare the shapes of the slow-rotator sequences in the Hyades and Praesepe and to determine whether they can be combined into a single benchmark sample for gyrochronology. Delorme et al. (2011) carried out a similar analysis. These authors compared P_{rot} distributions in the Hyades, Praesepe, and Coma Berenices (thought to be of similar age). Using a simple linear fit to the color-period relation, they found the Hyades to be ≈ 50 Myr older than the other two clusters. However, Delorme et al. (2011) did not have access to *Gaia* data for membership, nor did they have the wealth of new P_{rot} measurements enabled by *K2*'s observations of the Hyades and Praesepe. We use updated catalogs of rotators in both clusters to carry out our analysis.

Table 1. Literature Ages for the Hyades and Praesepe

	Hyades (Myr)	Praesepe (Myr)
Perryman et al. (1998)	625 \pm 50	...
Fossati et al. (2008)	...	590 $^{+150}_{-120}$
Brandt & Huang (2015a)	750 \pm 100	...
Brandt & Huang (2015b)	790 \pm 60	790 \pm 60
David & Hillenbrand (2015) ^a	827 $^{+10}_{-15}$...
	764 $^{+16}_{-17}$...
Choi et al. (2016)	...	630
Cummings et al. (2017)	635 \pm 25	670 \pm 25
Cummings et al. (2018) ^b	705 \pm 25	700 \pm 25
	705 \pm 25	685 \pm 25
Gossage et al. (2018) ^c	676 $^{+67}_{-11}$	617 $^{+40}_{-10}$
	741 $^{+55}_{-12}$	617 $^{+17}_{-15}$
	676 $^{+13}_{-30}$	589 $^{+13}_{-26}$
	589 $^{+29}_{-11}$	617 $^{+14}_{-13}$
Gaia Collaboration et al. (2018a)	794	708

^aDavid & Hillenbrand (2015) fit two different isochrone models; we give both results from their summed PDF analysis in log age space. ^bCummings et al. (2018) fit two different isochrone models; we list both results. ^cGossage et al. (2018) fit models with different rotation parameterizations to both (B,V) and (J,K_s) photometry. We give the results from fitting the model with a free rotation parameter and the model with a fixed rotation parameter but a spread in rotation to both color-magnitude diagrams.

We describe our membership and archival P_{rot} catalogs for the two clusters in Section 2 before deriving masses (M_*) and effective temperatures (T_{eff}) for these stars in Section 3. In Section 4, we identify binaries among our *K2* targets. Binary companions can impact the rotational evolution of a star, and therefore confuse interpretation of the mass-period distribution of a cluster. We then present new P_{rot} measurements for 116 Hyads from *K2* Campaign 13 in Section 5. Finally, we derive single-star sequences in both clusters using the second *Gaia* data release (DR2; Gaia Collaboration et al. 2018b), obtain a new reddening value for Praesepe, and derive a differential gyrochronological age for the Hyades in Section 6. We discuss our results and their potential implications for calibrating angular momentum evolution in Section 7, and conclude in Section 8.

2. EXISTING DATA

2.1. Hyades Membership and Rotation Catalog

As in Douglas et al. (2014, 2016), we use the Röser et al. (2011) and Goldman et al. (2013) catalogs as the

basis for our work. To these we add 13 stars identified using reduced proper motions and parallaxes from *Hipparcos*, bringing us to 786 total Hyads. Since archival data for the Hyades are generally of high quality, and since our pre-*Gaia* catalog was used to select our *K2* Campaign 4 and 13 targets (Guest Observer proposals 4095 and 13064), we do not attempt to update the full cluster membership list using *Gaia* DR2.

Furthermore, since our sample consists of variable stars and includes probable binaries, these stars will have increased photometric variability and possibly also high astrometric excess noise. This variability and excess noise will impact the availability of the *Gaia* data, as well as the determination of appropriate quality cuts. Indeed, 188 stars in our original catalog do not pass the quality cuts recommended by the *Gaia* Collaboration (Gaia Collaboration et al. 2018a), and >80 of these are confirmed or candidate binaries.

In Douglas et al. (2014, 2016), we assembled P_{rot} measurements for Hyads from Radick et al. (1987, 1995); Prosser et al. (1995); Delorme et al. (2011); Hartman et al. (2011); and from an analysis of All Sky Automated Survey (ASAS; Pojmański 2002) data (A. Kundert & P. Cargile, private communication, 2014)¹ into a catalog of 102 rotators. We then added 37 new P_{rot} from our analysis of *K2* Campaign 4 data in Douglas et al. (2016), bringing the total number of known Hyades rotators to 139. With a few exceptions, these surveys generally measure consistent P_{rot} ; for details, see Douglas et al. (2014, 2016). The mass-period relationship for these 139 Hyads is shown in Figure 1.

In the second half of this paper, we consider only single, slowly rotating Hyads, and we use *Gaia* data to select these stars. We match our Douglas et al. (2016) Hyades catalog to *Gaia* DR2, and select the nearest neighbor. We then check this match by computing synthetic *Gaia G* magnitudes from UCAC r, i magnitudes (Zacharias et al. 2010), SDSS r, i (Alam et al. 2015), 2MASS J, K (Skrutskie et al. 2006), and/or Tycho2 B, V (as given in 2MASS). We require that at least one of these synthetic magnitudes match the measured *Gaia*

¹ In Douglas et al. (2014) we cited these P_{rot} as Kundert et al. in prep, and in Douglas et al. (2016) as Cargile et al. in prep. These periods were measured by A. Kundert as an undergraduate while being supervised by co-author P. Cargile. The paper was never completed, however, and additional ASAS data have become available for Hyades members in the last few years. We therefore give the existing ASAS P_{rot} measurements in Table 3, but further details will be provided in a later paper, where we will re-analyze the expanded ASAS data set. Since we find that ground-based P_{rot} generally, and ASAS P_{rot} specifically, are consistent with *K2* periods, we feel justified in continuing to include the current ASAS periods in our analysis.

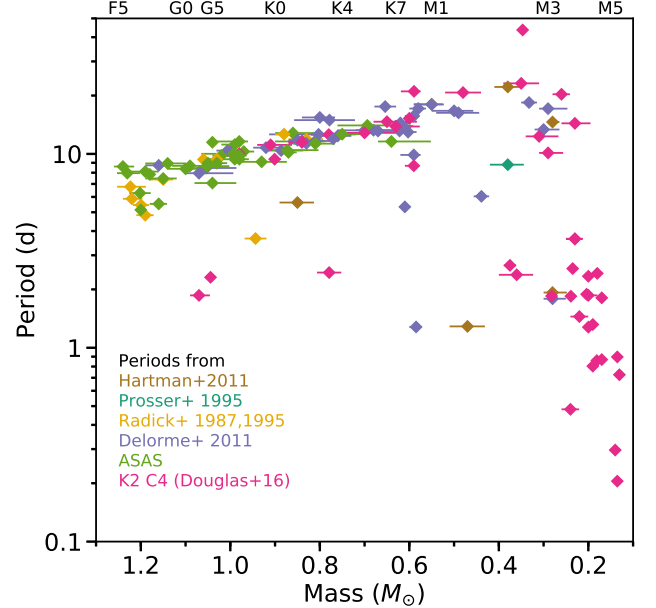


Figure 1. Mass-period distribution for Hyads with P_{rot} measurements in the literature. The color indicates the source of the P_{rot} . We also include the uncertainties on M_* , which are dominated by distance uncertainties even in the *Gaia* DR2 era. The error bars only represent systematic uncertainties from our mass calculation, and do not reflect, e.g., systematics in the model or excess K -band flux due to an unresolved companion.

G value to within 1 standard deviation (σ) for optical photometry or to within 2σ for 2MASS photometry. Of the 786 stars in our catalog, only 10 fail this test: three stars lack photometry to compute synthetic G magnitudes, two lack *Gaia* counterparts, and five fail the G magnitude test. However, none of those 10 stars has a measured P_{rot} or is a *K2* target, so they do not impact our analysis and are excluded from all tables.

2.2. Praesepe Membership and Rotation Catalog

We continue to use the Douglas et al. (2017) Praesepe membership catalog, which is based primarily on Kraus & Hillenbrand (2007). Our catalog includes 1130 cluster members with $P_{mem} \geq 50\%$ from Kraus & Hillenbrand (2007), supplemented by 39 previously cataloged members too bright to be identified by those authors. We assign these bright stars $P_{mem} = 100\%$.

In Douglas et al. (2014, 2017), we gathered P_{rot} measurements for Praesepe members from Scholz & Eisloffel (2007), Scholz et al. (2011), Delorme et al. (2011), Agüeros et al. (2011), and Kovács et al. (2014). We combined these literature values with 677 P_{rot} derived from our *K2* Campaign 5 data; in total, our catalog includes P_{rot} data for 743 Praesepe members.

We match this list of Praesepe rotators to *Gaia* DR2 and again select the nearest neighbor. Only three rotators in our catalog lack a DR2 match within 0°1: EPIC 211970974 and EPIC 211907026 are both rapidly rotating M dwarfs, and EPIC 211954582 is overluminous by −1.18 mag, which suggests that it might be a triple system. Since our analysis focuses on single, slowly rotating stars, the lack of a DR2 match in these three cases does not affect this work.

Five additional stars were mismatched when searching for the nearest neighbor, but in each case, another star was found within 0°1 with photometry consistent with our target:

Gaia DR2 661314466963687808 (EPIC 211971468),
Gaia DR2 659680072990872704 (EPIC 211903302),
Gaia DR2 661355934869899648 (EPIC 211983811),
Gaia DR2 663055371825360000 (EPIC 211981509),
Gaia DR2 661312267940341632 (EPIC 211966619).

3. DERIVED STELLAR PROPERTIES

3.1. Stellar Masses

As in previous work, we estimate stellar masses by linearly interpolating between the M_K and M_* points given by Kraus & Hillenbrand (2007), who list M_* and spectral energy distributions (SEDs) for B8–L0 stars.

We calculate distances (D) to individual stars using *Gaia* DR2 or *Hipparcos* (Perryman et al. 1998) parallaxes, or the secular parallaxes from Röser et al. (2011) or Goldman et al. (2013). For stars passing the *Gaia* quality cuts, we use *Gaia* parallaxes. For the remaining stars, we use *Hipparcos* parallaxes or secular parallaxes. We then use these distances to compute M_K .

We also propagate the m_K and D uncertainties for each star to determine the M_* uncertainties, σ_{M_*} . The uncertainties are typically small, on the order of a few percent. In our previous work, a few stars had large uncertainties in D , which led to large mass uncertainties. The improved parallaxes from *Gaia* have remedied this. Our stated σ_{M_*} are only the systematic uncertainties resulting from our calculation and the chosen model; they do not take into account other sources of uncertainty, such as our choice of model or K -band excesses due to a binary companion.

3.2. Effective Temperatures

In Section 6, we also compare the two clusters' P_{rot} – T_{eff} relations. For solar-type stars with $4700 < T_{eff} < 6700$ K, we derive an empirical color– T_{eff} relation using a *Gaia* DR2 match to the California Planet Survey catalog (Brewer et al. 2016). For warmer stars, we supplement this with Hyades members from *Gaia* Collaboration et al. (2018a) with T_{eff} from DR2/Apsis (Andrae

et al. 2018). For cooler stars, we combine the benchmark K and M dwarfs from Mann et al. (2015) and Boyajian et al. (2012). That sample only reaches $T_{eff} > 3056$ K, so we also adopt the Rabus et al. (2019) M_G – T_{eff} relation for stars with $2600 < T_{eff} < 4000$ K. At $T_{eff} = 4000$ K, our color– T_{eff} relation predicts a value only 9 K different from the Rabus et al. (2019) formula when using our fit to the Hyades main-sequence to convert between color and absolute magnitude.

4. BINARY IDENTIFICATION

We search binaries among known rotators in the Hyades because they can bias our analysis of the P_{rot} distribution. Binary companions may exert tidal or other physical effects on the primary star (e.g., Meibom & Mathieu 2005; Meibom et al. 2007; Zahn 2008; Douglas et al. 2016, 2017). In addition, when two (or more) stars are blended in a given image, the second star may dilute the rotational signal and/or add flux that will cause us to overestimate L_{bol} and M_* . These effects can cause stars to be misplaced in the mass–period plane, leading us to misidentify trends or transitions in the period distribution. Finally, short-period binaries are susceptible to tidal interactions, which can cause atypical angular momentum evolution. Binaries with orbital periods under ∼10 days might be circularized and locked, but others with orbital periods up to 30 days could still be affected. We therefore wish to identify as many binary systems as possible among our Hyades *K2* targets. We denote all confirmed and candidate binaries in our analysis, and provide a brief overview of our binary identification methods below. For more details, see Douglas et al. (2016, 2017).

1. *visual identification*: We examine a co-added *K2* image, a Digital Sky Survey (DSS) red image, and a 2MASS (Cutri et al. 2003) K -band image of each target to look for neighboring stars (see Figure 4). We use a flag of “Y” for yes, “M” for maybe, and “N” for no to indicate whether the target and a neighbor have blended point spread functions (PSFs) on the *K2* chip. Stars flagged as “Y” are labeled candidate binaries; we find 38 such targets, or 29% of stars with *K2* P_{rot} .

By searching 12 regions of the nearby sky in *Gaia* DR2, we find the rate of chance alignments with $G \leq 20$ mag stars within 10'' to be ≈6–58%. We find a range in potential contamination rates because the Hyades is so large on the sky: part of the cluster sits close to the Galactic Plane, but it also extends well away from the Plane. At typical Hyades distances, 10'' corresponds to ≈400–550 AU; it is possible that all of the blends we

Table 2. Confirmed and candidate multiple systems among **Hyades K2 targets and members** with Measured P_{rot}

[RSP2011] ^a	HIP	2MASS J	EPIC	D16	Updated	Gaia	Conf?	Ref
				Cand?	Cand?	Cand?		
323	...	04260584+1531275	...	N	N	N	Y	Patience et al. (1998); R. Stefanik (priv. comm.)
293	20577	04242831+1653103	...	Y	Y	N	Y	Douglas et al. (2014); Patience et al. (1998); Kopytova et al. (2016)
360	20899	04284827+1717079	...	N	N	N	Y	Mason et al. (2001)
329	20719	04262460+1651118	...	Y	Y	N	Y	Douglas et al. (2014); Mermilliod et al. (2009)
330	20741	04264010+1644488	...	N	N	N	Y	Morzinski (2011)
530	22203	04463036+1528194	...	N	N	N	Y	Morzinski (2011); R. Stefanik (priv. comm.)

NOTE—This table is available in its entirety in machine-readable form.

^a Index in the Röser et al. (2011) catalog

identify are chance alignments, or that up to 23% of Hyads have a companion within $\approx 400\text{--}550$ AU (for comparison, we determined that $\approx 10\%$ of Praesepe members likely have a bound companion within $10''$, or $10^3\text{--}10^4$ AU; Douglas et al. 2017). For consistency with our previous work, we continue to label probable blends as candidate binaries.

2. *photometric identification:* As in previous work, we identify candidate unresolved binaries that are overluminous for their color. In Douglas et al. (2014, 2016, 2017), we selected binaries that were overluminous in a rI vs $(rI - K_S)$ color-magnitude diagram (CMD), using *Hipparcos* Perryman et al. (1998) parallaxes or secular parallaxes from Röser et al. (2011) and Goldman et al. (2013). As in Section 3.1, we now update the rI vs $(rI - K_S)$ selection using *Gaia* DR2 parallaxes when the data passes the quality cuts defined in Gaia Collaboration et al. (2018a). We also select new photometric candidate binaries using *Gaia* DR2 photometry, discussed further in Section 6.1.2. This method is biased towards binaries with equal masses, and we are certainly missing candidate binaries with lower mass ratios. Our binary selections are shown in Figure 2; in Section 5 we flag all photometric candidate binaries, but in Section 6 we reject only candidates selected from *Gaia* photometry.

3. *multiperiodic K2 stars:* In binaries where the components have roughly equal brightness, variability from both stars can appear in the *K2* light curve. However, we may also detect two P_{rot} and/or an obvious beat pattern when a single star exhibits differential rotation. As discussed in Section 5, we assume that the two periods come from different components of a binary if the periods are different by $>20\%$. This cutoff is based on the maximum

period separation for differentially rotating spot groups on the Sun. We find multiple P_{rot} , indicating probable unresolved binaries, in 11 *K2* targets.

4. *literature identifications:* We searched the literature for Hyades binaries among known rotators and *K2* Campaign 4 targets in Douglas et al. (2016). We update this list with binaries among our Campaign 13 targets. We also add binaries identified or confirmed through observations with the Tillinghast Reflector Echelle Spectrograph (TRES) on the 1.5-m Tillinghast telescope at the Smithsonian Astrophysical Observatory’s Fred L. Whipple Observatory on Mt. Hopkins, AZ (R. Stefanik, private communication, 2018).

We consider all visual and photometric pairs, as well as multiperiodic *K2* stars, to be candidate binaries in our analysis. For other literature binaries, we follow the confirmed versus candidate nomenclature used in the source paper. The resulting list of confirmed and candidate binaries is given in Table 2.

5. MEASURING NEW HYADES ROTATION PERIODS WITH K2

5.1. *K2 Data and Initial P_{rot} Measurement*

K2 targeted the Hyades for a second time during its Campaign 13, which lasted from 2017 Mar 08 to 2017 May 27. We analyze the resulting long-cadence data for 132 Hyads identified in Section 2.1 and with *Kepler* magnitudes $K_p > 9$ mag and $M_* < 1.5 M_\odot$. These limits exclude saturated stars as well as stars with radiative outer layers, which are outside of the scope of this work. The distribution of Hyades targets in *K2* Campaigns 4 and 13 is shown in Figure 3.

We use detrended light curves generated using the *K2* Systematics Correction method (K2SC; Aigrain et al. 2016) for our analysis. Aigrain et al. (2016) developed a

Table 3. P_{rot} measurements for Hyades stars targeted in *K2* and in the literature

[RSP2011] ^a	EPIC	$P_{rot,1}$	Q_1 ^b	$P_{rot,2}$	Q_2 ^b	Multi ^c	Blend ^d	P^e	Radick	Prosser	HATnet	SWASP	ASAS	<i>K2</i> C4
		(days)		(days)					P_{rot} (days)					
549	248045685	40.10	2	N	N
544	247611242	11.79	0	N	Y	3
428	247369717	11.83	1	M	N	K	12.69	13.59	...
571	246865157	12.22	0	N	N	D	11.98
362	210554781	11.51	0	3.60	0	Y	N	R	3.66
409	246777832	12.90	0	N	N	D	13.13
553	246931087	10.81	0	N	Y	D	10.77
578	246732310	12.90	0	N	Y	D	13.14
355	210651981	2.45	0	1.07	1	M	Y	2	...	2.42	...	2.42	...	2.44
658	246806983	2.61	0	14.31	1	Y	N	D	14.94

NOTE—This table is available in its entirety in machine-readable form.

^a Index in the Röser et al. (2011) catalog

^b Quality of the P_{rot} detection. 0 is a high-confidence measurement, 1 is questionable, 2 is not trusted, and 3 indicates that there were no significant periodogram peaks.

^c Presence of multiple periods in the light curve. Y, M, and N represent “yes”, “maybe”, and “no”, respectively

^d Presence of a blended neighbor. Y, M, and N represent “yes”, “maybe”, and “no”, respectively

^e Flag for the P_{rot} source selected. “R”:Radick et al. (1987, 1995), “P”:Prosser et al. (1995), “H”:Hartman et al. (2011) (HATnet), “D”:Delorme et al. (2011) (SWASP), “A”:ASAS, “2”:Douglas et al. (2016) (*K2* Campaign 4), and “3”:this work (*K2* Campaign 13)

semi-parametric Gaussian process model to simultaneously correct for the spacecraft motion and model the stellar variability. As discussed in Douglas et al. (2017), we find that this approach is best at removing instrumental signals and trends while leaving stellar periodic signals intact.² We ran the K2SC code on the *K2* PDC pipeline light curves ourselves since the processed K2SC light curves for Campaign 13 are not yet on MAST. We downloaded the pipeline light curves in March 2018.

We follow the same period measurement method used in Douglas et al. (2017), and only summarize it here. We use the Press & Rybicki (1989) FFT-based Lomb-Scargle algorithm³ to measure P_{rot} . We compute the Lomb-Scargle periodogram power for 3×10^4 periods ranging from 0.1 to 70 d (approximately the length of the Campaign). We also compute minimum significance thresholds for the periodogram peaks using bootstrap re-sampling, and only consider a peak to be significant if its power is greater than the minimum significance threshold for that light curve. We take the highest sig-

nificant peak as our default P_{rot} value; only three of our targets show no significant periodogram peaks.

5.2. Period Validation

We employ several automated and by-eye quality checks to validate the P_{rot} identified above. We inspect each phase-folded light curve to confirm that the detected P_{rot} appears astrophysical and not instrumental. Clearly spurious detections are flagged as $Q = 2$, and questionable detections as $Q = 1$. A $Q = 3$ flag indicates that there were no significant periodogram peaks. Figure 3 in Douglas et al. (2017) shows examples of various light curve features, and describes how we flag them.

We also plot the full light curve with vertical dashed lines at intervals corresponding to the detected P_{rot} , to ensure that light curve features repeat over several intervals. Finally, we check for cases where there is a double-dip in the light curve, and the highest periodogram peak likely corresponds to half of the true P_{rot} . This is caused by two similar spot groups on opposite sides of the star. We then select the correct peak as the final P_{rot} .

Figure 4 shows an example of the plots we use to inspect the data; we include a figure set showing these plots for every target in our sample online.

We find 13 stars with significant periodogram peaks but no believable P_{rot} . In six cases, the light curve is just noise or displays only a long trend, without any detected periodic variability. In the remaining seven cases, there

² For more information, see Aigrain et al. (2016) and the MAST high level science product page, https://archive.stsci.edu/missions/hlsp/k2sc/hlsp_k2sc_k2_llc_all_kepler_v1_readme.txt.

³ Implemented as *lomb_scargle_fast* in the *gatspy* package; see <https://github.com/astroML/gatspy>.

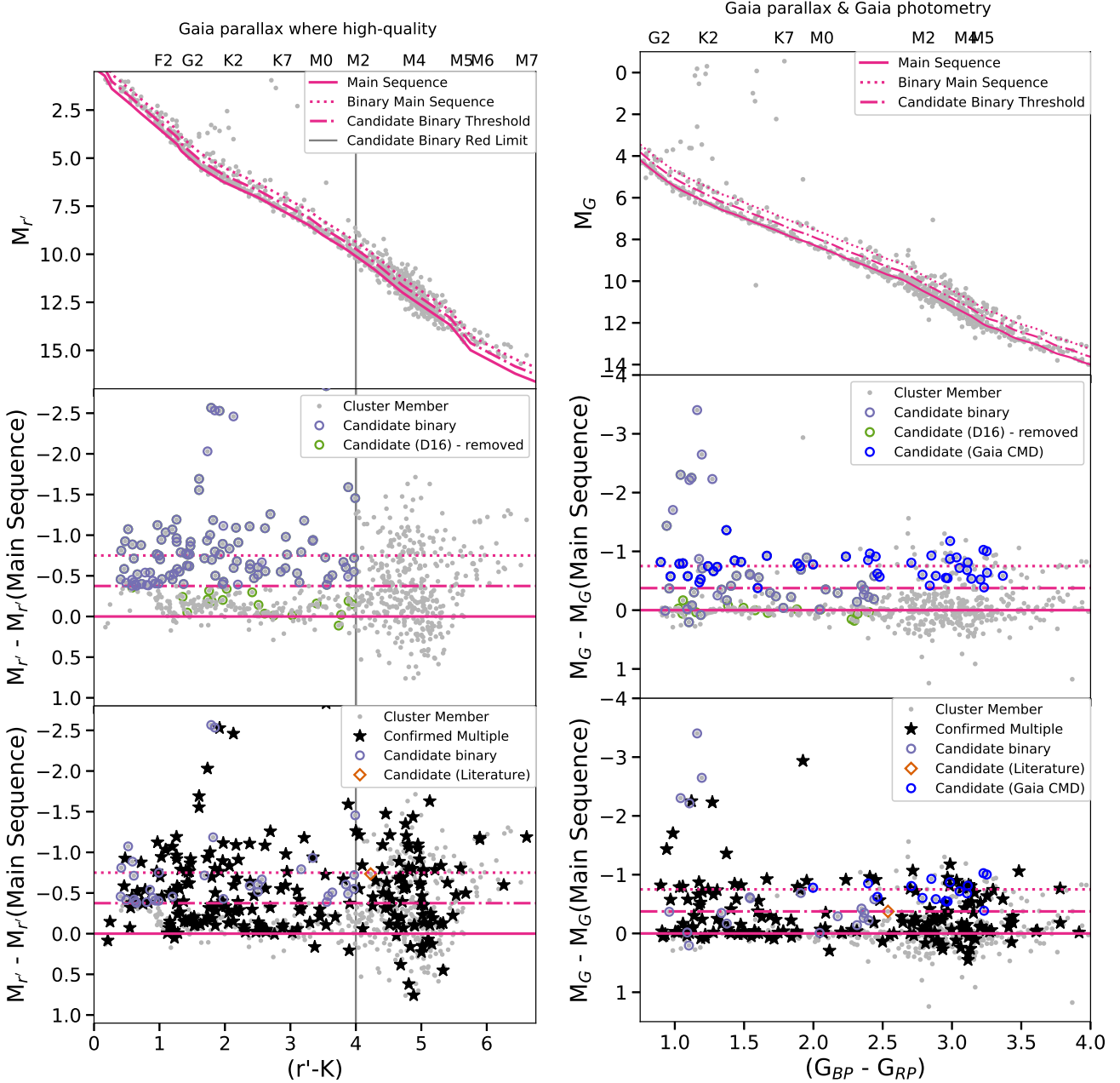


Figure 2. Demonstration of our photometric binary selection process. The left column shows the $(r' - K_s)$ color we used in previous work, but using *Gaia* parallaxes where available to determine $M_{r'}$. The right column shows one of the *Gaia* color-magnitude diagrams (CMDs) we used to update our candidate binary list for this work. *Top*—CMD with our selected main sequence (solid line) and binary cuts overlaid: the dotted line shows the nominal binary main sequence, and the dot-dashed line gives the minimum magnitude above which we consider a star to be a candidate binary. In previous work (left) we use the model SEDs assembled by Kraus & Hillenbrand (2007), and in this work (right) we use a polynomial fit to the Hyades main sequence. *Middle*—residuals between observed and expected absolute magnitudes; the horizontal lines are the same thresholds given above. Candidates identified in Douglas et al. (2016) are shown in green, and new candidates identified from *Gaia* DR2 photometry are given in blue. It is clear that the improved *Gaia* parallaxes have removed some of our previously identified candidate binaries. *Bottom*—the same as the middle panel, but now confirmed multiples (black stars) and literature candidates (orange diamonds) are also shown. While our photometric selection is useful for identifying additional candidates, there are still many confirmed binaries that show no photometric offset from the main sequence.

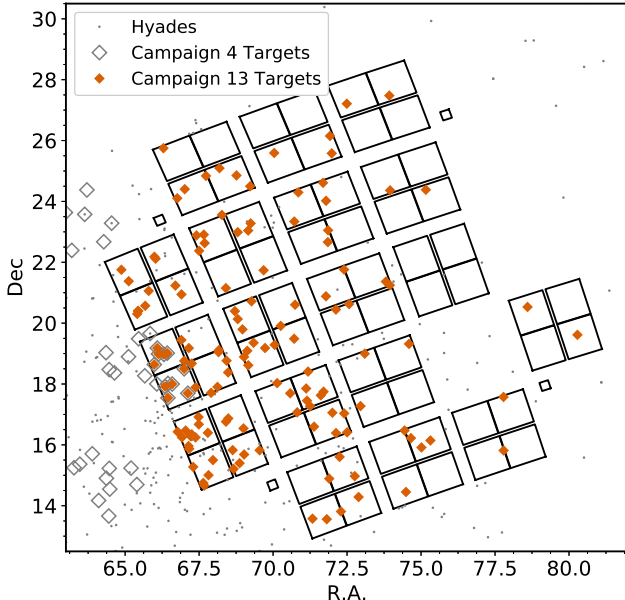


Figure 3. The *K2* Campaign 13 field of view, with our 132 Campaign 13 targets (orange diamonds), Campaign 4 targets (grey open diamonds), and other Hyads (grey dots). Three of the spacecraft’s detector modules are no longer functioning, but only a handful of Hyads would have fallen on these modules. Because the cluster is so large on the sky, many targets are near the edges of the field of view, and therefore have distorted PSFs.

is some probable spot-induced variability, but the phase-folded light curves do not actually match up and there is no clear period. In these cases, we are likely observing rapid spot evolution, perhaps on two stars in a binary.

For 18 other stars, the highest periodogram peak does not appear to correspond to the true P_{rot} . In some cases, as above, the highest periodogram peak comes from a campaign-long trend, and the true period is detected at a weaker power. In other cases, we find a double-dip light curve with almost no difference between the central (half-period) dip and the primary (full-period) dip. In these cases, the phase-folded light curve for the longer period shows the double-dip pattern clearly, even though it is detected at a lower periodogram power.

EPIC 210741091 and EPIC 247337843 are two very interesting cases: it is hard to define a period because the spot modulation only appears in half the campaign. For EPIC 210741091, there is initially some variability but no clear periodic signal; a V-shaped dip suggesting a single large spot (Bopp & Evans 1973; Eker 1994) appears about halfway through the campaign. Nonetheless, we measure $P_{rot} = 11.78$ d for this star, very close to the $P_{rot} = 11.98$ d value we measured in Campaign 4. EPIC 247337843 develops rapidly from cycle to cycle, from a slight double-dip at the beginning of the cam-

paign to variability with no clear period by the second half. Given this variability and partial lack of signal for both stars, we assign $Q = 1$ for their Campaign 13 P_{rot} .

Finally, in 11 light curves we detect two signals with periods differing by at least 20%. We consider these stars to be candidate binaries. Several other stars exhibit two close but distinct periodogram peaks, and the light curves have obvious beat patterns. This suggests that in these cases we are observing differential rotation of two spot groups at different latitudes.

5.3. Summary: New *K2* Periods for the Hyades

We obtain robust P_{rot} measurements for 116 Hyades members, including 93 members with no prior P_{rot} measurement. The vast majority of these periods are for rapidly rotating M dwarfs, and bring the total number of Hyades with P_{rot} to 232. Our P_{rot} values, flags, and analysis outputs are found in Table 3. Our new rotation periods, along with literature values, are shown as a function of stellar mass in Figure 5.

Only 23 stars have P_{rot} measured here and in previous studies, including five with a P_{rot} measurement from *K2* Campaign 4 (Douglas et al. 2016). Figure 6 shows a comparison of the existing data with our new measurements. In two cases (EPIC 210554781 and EPIC 246806983), the literature period is also detected as a secondary period in the *K2* light curve. In two other cases (EPIC 210558541 and EPIC 246714118), we detect a short P_{rot} in *K2* and do not detect the longer literature P_{rot} at all. In general, however, we find that ground- and space-based P_{rot} measurements agree to within 10%, similar to our results in Praesepe (Douglas et al. 2017).

6. COMPARING THE HYADES AND PRAESEPE

Based on the similarity of their color–magnitude diagrams (CMDs) and their activity, rotation, and lithium abundance data, the Hyades and Praesepe are often assumed to be coeval clusters (e.g., Douglas et al. 2014; Cummings et al. 2017). Here, we test this assumption using our expanded rotator samples paired with the high-precision data from *Gaia* DR2 for each cluster. First, we identify likely single-star members of each cluster. Then we apply a new gyrochronology model tuned with the Praesepe slow-rotating sequence and the Sun to infer a precise, relative, gyrochronological age for the Hyades.

6.1. Defining Single-Star Sequences

A comparison of Figure 5 and figure 7 in Douglas et al. (2017) shows that the color– P_{rot} distributions for the Hyades and Praesepe appear qualitatively similar to

EPIC 210491860

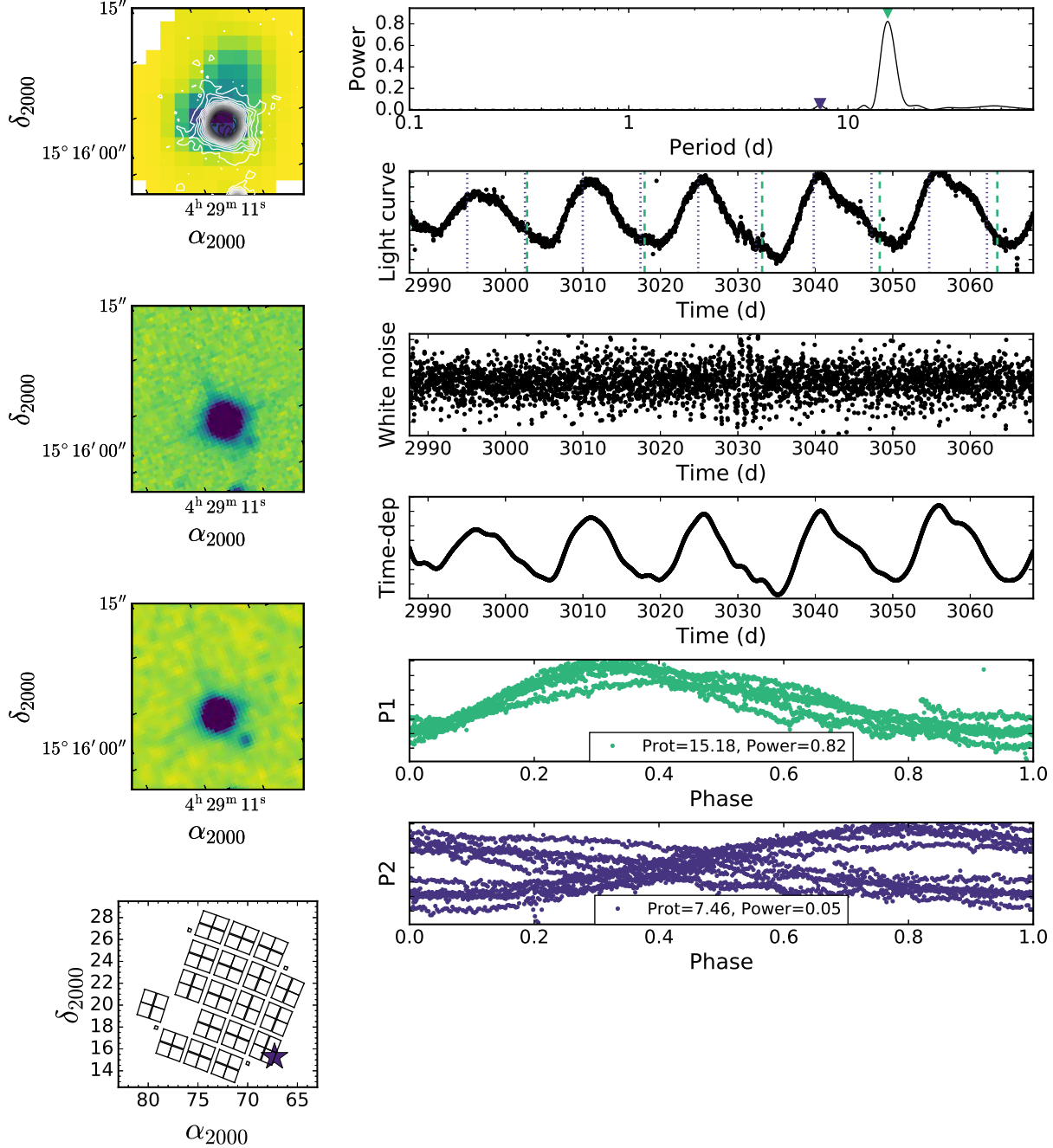


Figure 4. An example of the plots used to inspect period detections and check for neighboring stars. *Left column, top to bottom*—*K2* pixel stamp with DSS Red image overlaid as a contour; DSS Red image rotated into the *K2* frame; 2MASS image rotated into the *K2* frame; and the target’s position within the *K2* Campaign 13 field of view. A faint companion is visible in both the DSS and 2MASS images. *Right column, top to bottom*—Lomb-Scargle periodogram with (up to) the three highest significant peaks indicated by inverted triangles; the light curve corrected for spacecraft drift; the white-noise component of the light curve; the time-dependent component; and the light curve phase-folded on (up to) the three most significant periods. The colors of the markers indicating the peaks in the periodogram correspond to the colors of the phase-folded light curves. Slight spot evolution is apparent, and the *K2SC* algorithm struggles around the middle of the campaign. Versions of this plot for every *K2* target analyzed are available as an electronic figure set.

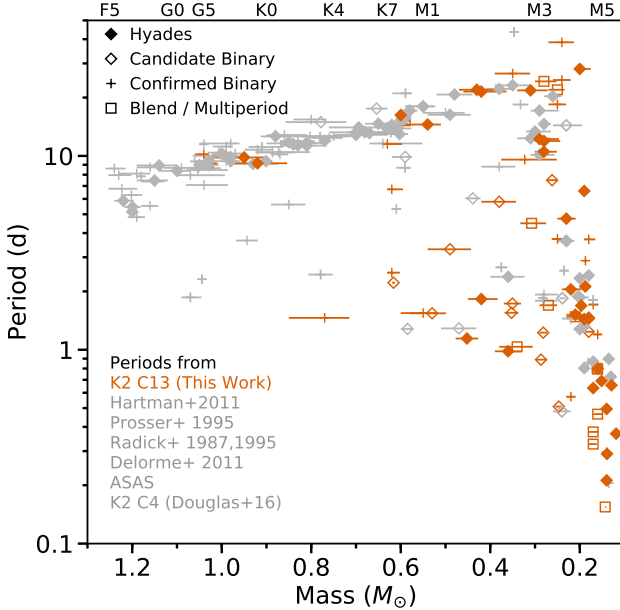


Figure 5. Hyades mass– P_{rot} plane showing literature (grey) and new high-quality $K2$ (dark orange) P_{rot} . We also mark confirmed and candidate binaries: plusses indicate confirmed binaries, open diamonds indicate photometric or spectroscopic candidate binaries, and open squares indicate $K2$ targets with a blended neighbor or a second period in the light curve. Approximate spectral types are indicated along the top. All rapidly rotating stars with spectral types earlier than \sim K5 are confirmed binaries.

each other. Most stars follow a common slow-rotator sequence from the late-F stars down to early M, followed by a sharp transition from slow to rapid near the fully convective boundary at \approx M4. However, many stars are outliers and appear to be rotating more rapidly or slowly than the slow-rotating sequence.

Where possible, it is important to reject outliers following membership and multiplicity criteria, instead of removing them based on their position in color–period space. The primary reason is that we wish to show that \approx 700-Myr-old stars follow a single-valued color– P_{rot} relation from mid-F down to early M, and that any rapid stars in this mass range are rapid for a reason unrelated to single-star angular-momentum evolution (e.g., because they are binaries, blends, or interlopers, or have poor data). Since the Hyades and Praesepe samples of rotators are large, we can apply strict physical (e.g., based on positions, kinematics, or luminosity excesses) and data-quality criteria (e.g., poor astrometric solutions, blended light curves resulting in multiple period detections) to select stars with *Kepler* and *Gaia* data consistent with single-star membership without overdepleting the color–period plane at any color. We describe our selection criteria below; each criterion is ap-

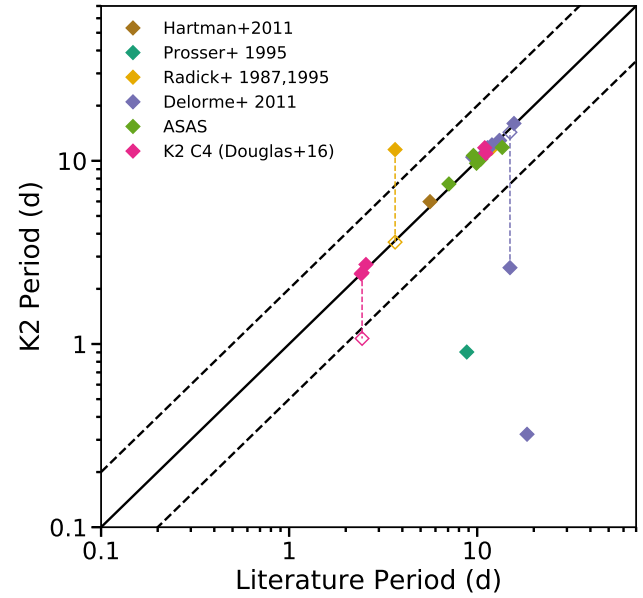


Figure 6. Comparison between the literature P_{rot} and that measured from $K2$ Campaign 13. Solid diamonds represent the primary period we detect in $K2$ Campaign 13 data, while open diamonds represent the secondary period, if any. In two cases, the literature period was detected at lower significance in the $K2$ light curve. Overall, we find good agreement between $K2$ campaigns and between $K2$ and ground-based studies.

plied independently and the outputs combined to create our final list of single members. The results are summarized in Figure 7, and Tables 3 and 4 include flags indicating which tests were passed by each star

6.1.1. Kinematics

For the Hyades, we select candidate single stars first by rejecting confirmed binaries identified in the literature, and then by considering the Galactic UVW space velocities for stars with six-parameter positions and kinematics from *Gaia* DR2. We calculate the cluster median UVW velocities from the Hyades membership list in [Gaia Collaboration et al. \(2018a\)](#);⁴ next, we compute the absolute velocity deviation, Δv , for the 101 rotators in our sample with six-parameter positions and kinematics by subtracting off the cluster median values for each UVW component and then adding the residuals in quadrature. The Hyades’s internal velocity dispersion is estimated to be only 0.3 km s^{-1} ([Gunn et al. 1988](#); [Perryman et al. 1998](#)), which is comparable to the DR2 radial velocity (RV) error. We adopt a more conservative threshold for identifying non-single members of $\Delta v > 2 \text{ km s}^{-1}$, which eliminates 26 stars. We also con-

⁴ For the Hyades, $(U, V, W) = (+42.3, -19.2, -1.2) \text{ km s}^{-1}$.

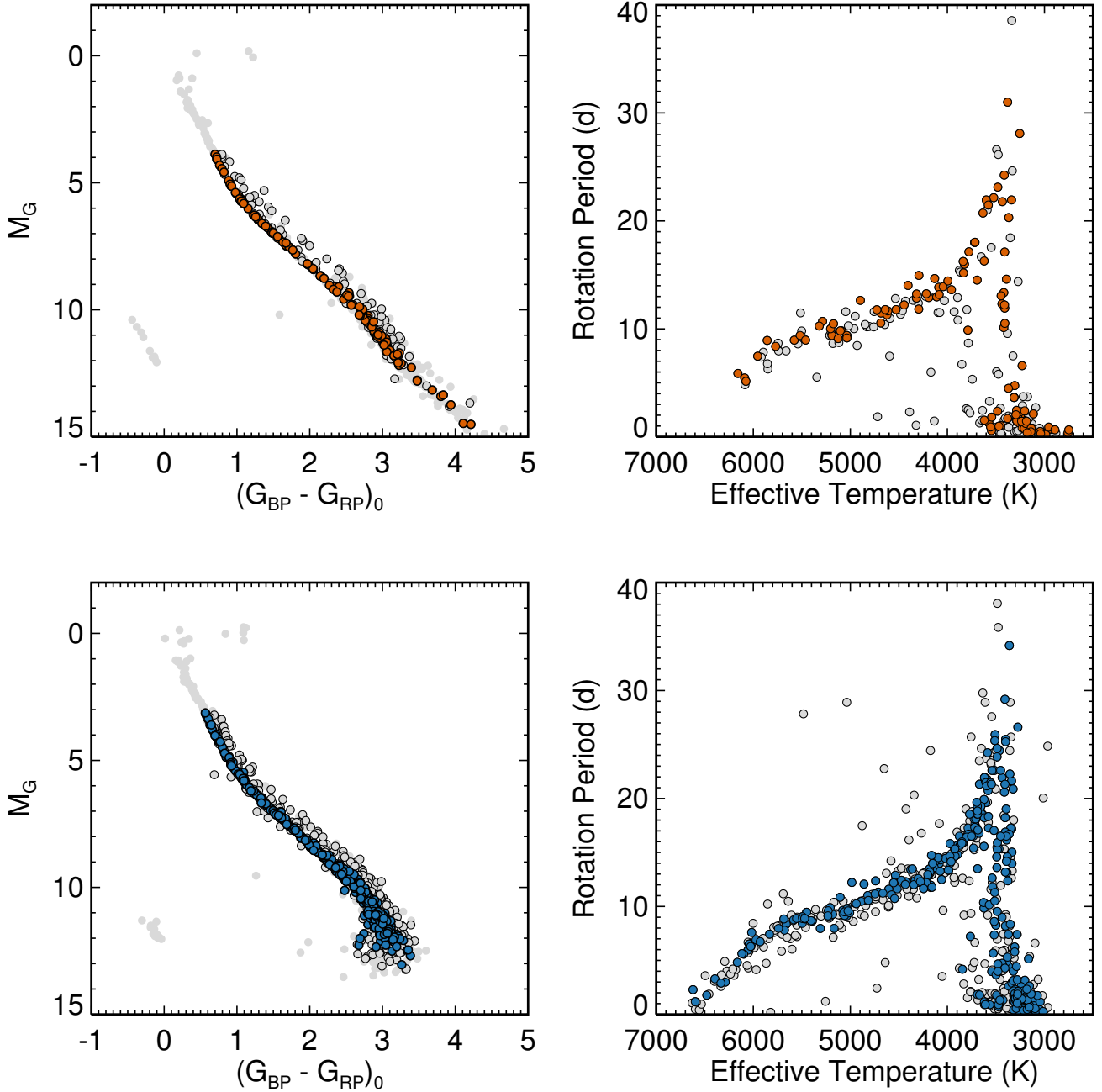


Figure 7. CMDs (left column) and P_{rot} distributions (right column) for the Hyades (top row) and Praesepe (bottom row). Top left—[Gaia Collaboration et al. \(2018a\)](#) Hyades members are plotted as gray points, stars with measured P_{rot} are gray points outlined with black circles, and the subset we identify as single-star members are shaded orange. Top right— P_{rot} for the Hyades are plotted against T_{eff} , which we calculated from *Gaia* DR2 photometry using empirical color–temperature relations described in Section 3.2. Filtering out rotators that are known spectroscopic binaries, or have multiple periods detected in *K2* light curves, or are astrometric or photometric non-single members from *Gaia* DR2 removes all rapid outliers from the diagram, revealing a cleanly converged slow sequence down to $T_{eff} \approx 3500$ K. Bottom left—[Gaia Collaboration et al. \(2018a\)](#) Praesepe members are plotted as gray points, stars with P_{rot} are gray points outlined with black circles, and the subset we consider to be single-star members are shaded blue. Bottom right—Applying similar filtering as described for the Hyades removes all slow outliers in Praesepe’s P_{rot} distribution, and all rapid outliers down to $T_{eff} \approx 4000$ K. The slow sequence appears converged down to $T_{eff} \approx 3600\text{--}3800$ K, depending on the still uncertain multiplicity of a few rapid stars in that range.

sider stars with DR2 RV errors $\sigma_{RV} > 2 \text{ km s}^{-1}$ to be non-single members, which cuts an additional four stars, so that in the end we have 71 single-star rotators in our sample.

For Praesepe, we first remove the 43 binaries confirmed in the literature. Then, we filter non-single-member stars using proper motions separately from RVs. This is possible because Praesepe is more distant than the Hyades and useful because 719 of 743 rotators have DR2 proper motions, whereas only 185 have DR2 RVs. The distribution of proper motions for our rotator sample can be approximately described by a Gaussian with $\sigma = 1.25 \text{ mas yr}^{-1}$ (the median proper motion error is 0.2 mas yr^{-1}). We set our threshold at twice this value and reject stars with absolute proper motion deviations larger than this 2.5 mas yr^{-1} .⁵ This eliminates 146 of 719 stars with DR2 proper motions. Separately, we reject 48 stars with $\Delta RV > 2 \text{ km s}^{-1}$ from the cluster median value quoted by [Gaia Collaboration et al. \(2018a\)](#),⁶ and 46 stars with $\sigma_{RV} > 2 \text{ km s}^{-1}$. In total, we reject 196 unique non-single members, and retain 523 single-star rotators.

6.1.2. Photometry

We use the [Gaia Collaboration et al. \(2018a\)](#) Hyades catalog to generate a fiducial cluster CMD, and then iteratively fit the resulting main-sequence with a cubic basis-spline. We then generate a new CMD using our full rotator list, and determine each star's deviation from the fiducial main-sequence.

We fit two CMDs: absolute G magnitude, M_G , versus both $(G_{\text{BP}} - G_{\text{RP}})$ and $(G - G_{\text{RP}})$. We analyze $(G - G_{\text{RP}})$ to account for the larger uncertainty in G_{BP} for redder/fainter stars. We then calculate the photometric deviation from these empirical main-sequences for our rotator sample, $d_{cmd} = |M_{G,\text{observed}} - M_{G,\text{predicted}}|$, and label all stars that are consistent with at least one of the empirical isochrones as photometric single-member stars. We set a threshold of $d_{cmd} < 0.375 \text{ mag}$ for all stars, which is half of the offset for an equal-mass binary (e.g., [Hodgkin et al. 1999](#)). We find that 176 of 222 Hyads with DR2 photometry are consistent with being single-star members.

For Praesepe, we adjust the fiducial Hyades CMD fit according to its interstellar reddening/extinction that we derive in Appendix A ($A_V = 0.035$) and the distance modulus implied by inverting the cluster parallax ($\varpi = 5.371 \text{ mas}$; [Gaia Collaboration et al. 2018a](#)). We find

⁵ For reference, a 0.5 km s^{-1} velocity dispersion at the distance of Praesepe (186 pc) translates to $\approx 0.57 \text{ mas yr}^{-1}$.

⁶ For Praesepe, $\mu_\alpha \cos \delta, \mu_\delta = \{-36.047, -12.917\} \text{ mas yr}^{-1}$.

525 of the 741 stars with DR2 photometry are consistent with being single-star members.

6.1.3. Astrometric data quality

The *Gaia* DR2 astrometric solution for each star assumes it is a single point source. Objects that are inconsistent with this assumption can have excess astrometric noise (ϵ_i), and we remove those with $\epsilon_i > 1$ and $G < 19 \text{ mag}$ from our samples. This includes 40 stars in the Hyades and 48 stars in Praesepe. Most were already filtered by our kinematic and photometric selection criteria.

6.1.4. P_{rot} quality and corrections

For rotators with $K2$ light curves, we remove those for which we detect multiple periods, which, again, we interpret as either physically unassociated blends or cluster binaries (see Sections 4 and 5.2).

For Praesepe, an additional step is required: several periods in the literature need to be corrected. In [Douglas et al. \(2017\)](#), we assembled literature periods and our own $K2$ periods, and then recommended which source to use for each star. We recommended [Delorme et al. \(2011\)](#) for EPIC 211995288, and [Scholz & Eislöffel \(2007\)](#) for EPIC 211970147 (K2-102; [Mann et al. 2017](#)). But after re-inspecting the $K2$ light curves, it is clear that our $K2$ periods are accurate and the literature values are half-period harmonics.

The Campaign 5 light curves for EPIC 211890774 and EPIC 211822797 (K2-103; [Mann et al. 2017](#)) both show weak asymmetries in the depths of alternating minima, which we confirm with their Campaign 16 light curves. This indicates that the [Douglas et al. \(2017\)](#) measurements for these two stars are half-period harmonics, caused by presumably by nearly symmetric spot patterns on opposite-facing hemispheres. We therefore double the old P_{rot} for these stars.

Finally, EPIC 211950227 was originally given a period of 13.15 d ([Delorme et al. 2011](#)). However, the Campaign 16 light curve shows that the dominant modulation signal has a period of $P_{\text{rot}} = 1.76 \text{ d}$. We see no $\approx 13 \text{ d}$ signature in its Campaign 16 light curve and conclude that the $K2$ -derived P_{rot} is the correct one.

6.2. Resulting CMDs and $T_{\text{eff}}-P_{\text{rot}}$ Distributions for the Hyades and Praesepe

The resulting CMDs for the two clusters are shown in the left column of Figure 7, with their $T_{\text{eff}}-P_{\text{rot}}$ distributions in the right column. Applying the cuts described above yields a nearly clean P_{rot} distribution for both clusters. Overall, 118 Hyades rotators out of 232 satisfy our single-star-membership criteria. When examining the cluster's P_{rot} distribution, we find no rapid outliers

Table 4. Praesepe stars with measured P_{rot}

2MASS	EPIC	P_{rot} (d)	P ^a	T_{eff}	DR2Name ^b	SingleFlag
...	212004731	3.96	2	6196.83	661438260802777984	NYYNN
...	211930461	14.59	2	4019.60	661211147230556032	YYYYNN
08410747+2154567	212094548	6.60	2	3097.71	665178391340402944	YYY-Y
08395507+2003542	211988287	3.29	2	6395.48	664327433763175040	YYYYYY
08400063+1948235	211971871	2.99	K	6289.11	661311752544248960	YYY-Y
08400130+2008082	211992776	1.18	2	6597.70	664328915529294976	YYY-Y
08402232+2006244	211990908	2.59	K	6333.77	661419259867454976	YYNYN
08401763+1947152	211970750	6.69	K	6054.54	661310790468509952	-NY-Y

^a Flag for the P_{rot} source selected. “S”:[Scholz & Eislöffel \(2007\)](#); [Scholz et al. \(2011\)](#), “P”:[Agüeros et al. \(2011\)](#) (PTF), “D”:[Delorme et al. \(2011\)](#) (SWASP), “K”:[Kovács et al. \(2014\)](#) (HATnet), “2”:[Douglas et al. \(2017\)](#) (K_2 Campaign 5), and “16”: this work (K_2 Campaign 16; see Section 6.1.4)

^b Flags for selecting single stars in Section 6.1. Entries correspond to astrometry, photometry, K_2 multiperiodic, RV, and confirmed binary selection: “Y” indicates the star passes a given test, “N” indicates failure, and “-” indicates that we lack the data to perform a particular test. We only retain stars flagged “YYYYYY” or “YYY-Y”.

relative to the cleaned, slow-rotating sequence for $M_\star \gtrsim 0.57 M_\odot$ ($T_{eff} \gtrsim 3789$ K), and only three moderately faster rotators for $M_\star \gtrsim 0.5 M_\odot$ ($T_{eff} \gtrsim 3620$ K). The transition to completely rapid rotation in the Hyades occurs at $M_\star \approx 0.35 M_\odot$ ($T_{eff} \approx 3420$ K, M3), which is slightly warmer than the T_{eff} –radius discontinuity at $T_{eff} = 3200$ –3340 K identified by [Rabus et al. \(2019\)](#).

For Praesepe, we find that 496 of the 743 rotators are consistent with being single-star members. None of these stars appears significantly more rapid than the slow converged sequence for $T_{eff} \gtrsim 3845$ K ($M_\star \gtrsim 0.6 M_\odot$, M0). Of the 43 single members on our list with $3600 < T_{eff} < 3850$ K, 10, or 23%, are rapidly rotating outliers that have P_{rot} faster than the slow sequence by at least 3 d. The transition to all rapid rotators happens around $M_\star \approx 0.4 M_\odot$ ($T_{eff} \approx 3500$ K), but is not as well defined as in the Hyades.

Finally, Pr0211 (EPIC 211936827, *Gaia* DR2 661222279785743616) hosts a hot Jupiter ($M_p \sin i = 1.844 M_{Jup}$, $P_{orb} = 2.15$ d; [Quinn et al. 2012](#)). We find that Pr0211 rotates 1.4 d (15%) faster than expected, in agreement with [Kovács et al. \(2014\)](#)

6.3. A Precise Differential Gyrochronology Age for the Hyades

We now turn to the question of whether Praesepe and the Hyades are truly coeval. We search the literature and tabulate recent isochrone ages for the two clusters derived using a variety of photometry, constraints, models, and methods (see Table 1). From these, we calculate an age for the Hyades of 728 ± 71 Myr (median and 1σ of thirteen values), and for Praesepe of 670 ± 67 Myr (median and 1σ of eleven values). Since this suggests that Praesepe is the younger of the two clusters, we then calibrate an empirical gyrochronology model by fit-

ting the Praesepe T_{eff} – P_{rot} sequence, and then tune the age-dependence with the Sun. Finally, we compare the T_{eff} – P_{rot} sequences of the Hyades and Praesepe, and derive a precise, differential age according to our empirical model.

We summarize our assumed values for the Sun here. We take the Sun’s $P_{rot} = 26.09$ d, measured from periodic modulations in the Mount Wilson Ca II H & K S-index by [Donahue et al. \(1996\)](#). We take its age to be $4567 \pm 1 \pm 5$ Myr ([Chaussidon 2007](#)). Based on observations of solar twins derived from the updated Spectroscopic Properties of Cool Stars (SPOCS; [Brewer et al. 2016](#)) catalog, we derive a solar color of $(G_{BP} - G_{RP})_\odot = 0.817$ mag, consistent with the value of $(G_{BP} - G_{RP})_\odot = 0.82$ estimated by [Casagrande & Vandenberg \(2018\)](#). A more detailed discussion of our derivation of this color can be found in Appendix B.

Our analysis also makes the following assumptions:

1. The Sun has slowed down continuously since it was 670 Myr old (our adopted age of Praesepe). According to [van Saders et al. \(2016\)](#), magnetic braking efficiency plummets at a critical Rossby number (the ratio of P_{rot} to convective turnover time) of $R_{crit} = 2$, approximately the current solar value. We assume that the Sun has not yet reached this threshold and that it has therefore spun down continuously with a single-valued time dependence.
2. The difference in metallicity between the Sun and Praesepe does not appreciably affect spin-down and that comparing equal-color stars is valid, even

though a solar-mass star in Praesepe is cooler than the Sun’s current temperature.⁷

We fit a sixth order polynomial to Praesepe’s cleaned and dereddened DR2 color–period sequence for stars with $((G_{BP} - G_{RP})) < 2.4$ ($T_{\text{eff}} \approx 3500$ K, $M_{\star} \approx 0.42 M_{\odot}$, M2V). This color limit stops our model before the sharp drop to rapid rotation around the fully convective boundary. The sixth order polynomial is necessary as lower-order polynomials fail to accurately track the rapid change in P_{rot} from the F to G dwarfs. The final polynomial we use is

$$\begin{aligned} P_{\text{rot}} = & -330.81006 \\ & + 1462.4834(G_{BP} - G_{RP}) \\ & - 2569.3547(G_{BP} - G_{RP})^2 \\ & + 2347.1326(G_{BP} - G_{RP})^3 \\ & - 1171.8965(G_{BP} - G_{RP})^4 \\ & + 303.61984(G_{BP} - G_{RP})^5 \\ & - 31.922667(G_{BP} - G_{RP})^6 \end{aligned} \quad (1)$$

The Praesepe fit predicts a period at the solar color of $P_{\text{rot}} = 8.09 \pm 0.25$ d. We calculate this value using a $T_{\text{eff}} - P_{\text{rot}}$ diagram de-reddened by our $A_V = 0.035$ value, while the uncertainty comes from assuming either $A_V = 0$ (no reddening) or $A_V = 0.084$ (Taylor 2006). We use the age for Praesepe derived from the literature of 670 Myr, and calculate that the braking index $n = 0.619$.

We now apply our new gyrochronology formula to the cleaned stars in the Hyades with $0.7 < (G_{BP} - G_{RP})_0 < 1.1$, where gyrochronology should be viable at this age (Agüeros et al. 2018, Curtis et al. in prep.). If Praesepe is 670 Myr old and its $A_V = 0.035$, and if it is chemically identical to the Hyades, then the Hyades is 57 Myr older. We find the Hyades age to be 727 ± 75 Myr (median and 1σ), based on 25 cluster members. (For 49 analogous Praesepe stars, $1\sigma = 69$ Myr.) Recall that we calculate an isochrone age difference of 58 Myr by computing

⁷ Stars do not spin down through $T_{\text{eff}} - P_{\text{rot}}$ space along perfectly vertical lines, since they warm as they age. Differences in metallicity will also modify moments of inertia, convective turnover times, and other physical ingredients that are critical to understanding angular-momentum evolution. Theoretical models are the appropriate way of accounting for metallicity and stellar-evolution effects (e.g., van Saders & Pinsonneault 2013), but we presently lack sufficient coeval benchmarks with different metallicities to validate their predictions. Also, all available models fail to represent the cluster sample, aside from the most Sun-like G dwarfs (e.g., Agüeros et al. 2018, Curtis et al. submitted, and this work). Since our primary goals are to test if the Hyades and Praesepe are truly coeval and to measure a differential age, any systematic inaccuracies in the model will propagate to both cluster ages equally.

the difference between the median of various isochronal ages for each cluster; this is essentially identical to our differential gyrochronology result.

Figure 8 shows the $T_{\text{eff}} - P_{\text{rot}}$ diagram for the cleaned Praesepe and Hyades samples, and their corresponding gyrochronology ages using our recalibrated formula. Derived ages for individual stars are given in Table 6.

7. DISCUSSION

New P_{rot} measurements from *K2* and precise *Gaia* data have enabled us to compare the rotation distributions in Praesepe and the Hyades in detail. Whereas in previous work we assumed that the clusters have overlapping P_{rot} sequences, we now find that is not the case for solar-type stars. Overall, we find that Hyades FG stars rotate more slowly than their Praesepe counterparts, corresponding to a differential gyrochronological age of 57 Myr. This difference is consistent with the 47 ± 17 Myr difference between the clusters found by Delorme et al. (2011), who used a linear fit to the P_{rot} vs. $(J - K_s)$ relation in the Hyades and Praesepe. The 57 Myr age difference suggests that the two clusters should be separated when considering the evolution or effects of stellar rotation in solar-type stars and when accuracy below the 10% level is required.

Interestingly, the age discrepancy between the two clusters is largest for $T_{\text{eff}} > 5200$ K and decreases as we move to cooler stars. We fit the gyrochronology ages of Hyades stars with locally weighted scatterplot smoothing (LOWESS) as a function of T_{eff} , and compare it to the fiducial Praesepe model (Figure 9). Between $5250 > T_{\text{eff}} > 4900$ K, the differential gyro ages decrease, so that cooler Hyads converge with the Praesepe sequence. The late K and early M dwarfs do not brake appreciably from the age of Praesepe to that of the Hyades. This contradicts the common assumption that braking timescales increase as mass decreases. Our work therefore adds to prior evidence that low-mass stars follow a different, more complex braking timeline than their solar-type counterparts.

Several other authors have reached similar conclusions. Meibom et al. compared M35 (≈ 150 Myr; Meibom et al. 2009), M34 (≈ 220 Myr; Meibom et al. 2011a), and NGC 6811 (≈ 1 Gyr; Meibom et al. 2011b) to the Hyades, and find that K dwarfs must spin down less efficiently than FG stars. Cargile et al. (2014) found the same result by comparing Blanco 1 and the Pleiades (both ≈ 125 Myr) to M37 (≈ 550 Myr), the Hyades, and NGC 6811. Similarly, Agüeros et al. (2018) found evidence for stalling from the age of Praesepe to that of NGC 752 (≈ 1.3 Gyr) for K and early M stars. Finally, Curtis et al. (submitted) re-examined NGC 6811

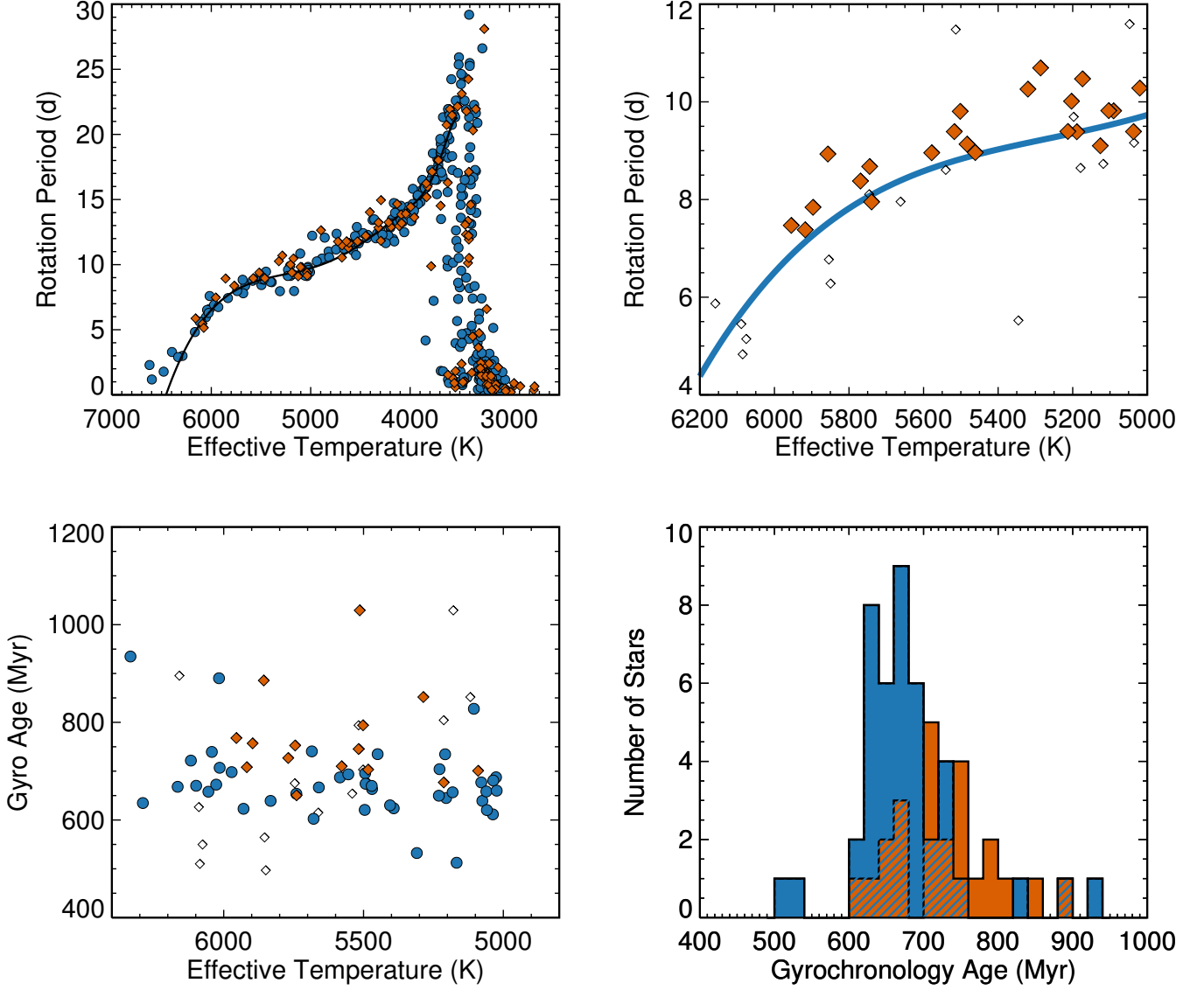


Figure 8. *Top left*—The T_{eff} – P_{rot} distributions for likely single stars in Praesepe (blue circles) and the Hyades (orange diamonds). The black line is a polynomial fit to the Praesepe stars with $0.65 < (G_{BP} - G_{RP})_0 < 2.4$. The distributions for the two clusters appear roughly consistent. *Top right*—Rotation data for single Hyads (orange diamonds) used in the gyrochronology age calculation ($5000 < T_{\text{eff}} < 6000$ K). Non-single Hyads (open diamonds) are shown for comparison. Single Hyads rotate systematically more slowly than the Praesepe polynomial model (blue line). *Bottom left*—Gyrochronology ages for the single Praesepe (blue circles above) and Hyades (orange diamonds above) samples over the range in T_{eff} where gyrochronology should be viable at this age (Agüeros et al. 2018). These Hyads are systematically older than the Praesepe stars (adopted age of 670 Myr) by ≈ 57 Myr. *Bottom right*—A histogram of the data in the scatter plot in the previous panel. The age distributions overlap, but the Hyades sample is systematically older by 57 Myr. Having large samples of stars helps mitigate the uncertainties for individual stars that caused the apparent age spreads (whether due to P_{rot} measurement uncertainties or intrinsic spread) for age-dating coeval populations.

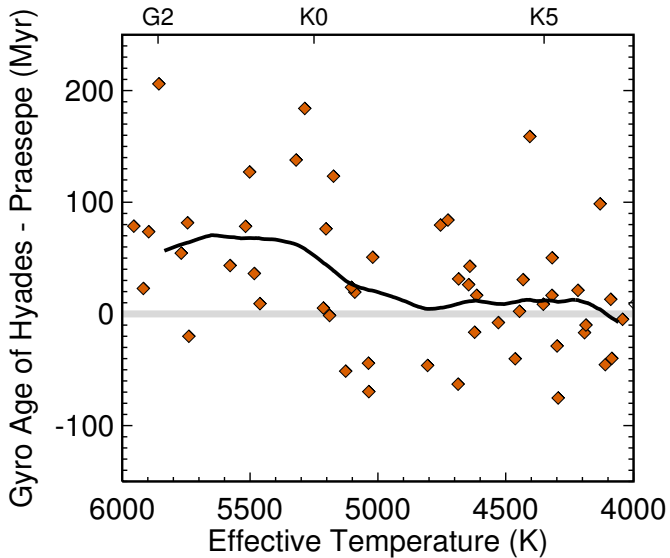


Figure 9. The differential gyrochronology ages for individual Hyads (orange diamonds) compared to our fiducial Praesepe model (grey horizontal line). We also show the LOWESS regression for the age difference, showing that the difference in gyrochronology ages is strongest for G stars, and decreases between $5250 > T_{\text{eff}} > 4900$ K until the cooler Hyads appear coeval with their cousins in Praesepe.

by searching *Gaia* DR2 for additional members with *Kepler* light curves, thereby significantly expanding the size of that cluster’s rotator sample and extending it down in mass from $M_{\star} \approx 0.8 M_{\odot}$ to $\approx 0.6 M_{\odot}$. Surprisingly, these authors found that NGC 6819’s slow rotator sequence converges with that of the Hyades and Praesepe at redder colors, indicating that these stars effectively do not spin down at all over a time span of several 100 Myr.

We therefore provide concrete evidence that K stars spin down at a variable rate, as opposed to existing empirical models which show them spinning down continuously from the time they reach the main sequence. This stalling is apparent even over ~ 50 Myr timescales. Previous empirical work has assumed a fixed functional form for the dependence of P_{rot} on mass or $(B - V)$ at all ages. For example, Delorme et al. (2011) fit a line to the P_{rot} vs. $(J - K_s)$ distributions in clusters, and Barnes (2003, 2007) fit other analytic functions. These efforts assumed that it was possible to decouple the mass and age dependencies, but our results demonstrate that rotation evolves at different rates for stars of different masses.

Barnes (2010) presented the only empirical gyrochronology relation that allowed more complicated mass-dependent evolution by including a dependence

on the convective turnover time τ , instead of color. That model accurately described the $M_{\star} > 0.85 M_{\odot}$ stars in the 2.5 Gyr NGC 6819 cluster (Meibom et al. 2015). However, it actually predicted that K dwarfs spin down more rapidly than G dwarfs, instead of more gradually as indicated by the open cluster data. Mamajek & Hillenbrand (2008), Meibom et al. (2009), and, more recently, Angus et al. (2015) simply re-calibrated the model presented by Barnes (2003, 2007), without considering more complex mass-dependent rotational evolution.

One probable reason that empirical models have not included a mass dependence is the paucity of $\gtrsim 1$ -Gyr-old benchmarks for K and M dwarf rotators. P_{rot} have been published for solar-type members of NGC 6819 and M67, but not their lower-mass members. We show that this dependence is present even over short timescales, but the field of gyrochronology requires additional benchmarks at older ages to properly calibrate braking timescales for stars of different masses. Future work on NGC 6819 and Ruprecht 147, also ≈ 2.5 Gyr old, will provide further constraints on mass-dependent evolution at older ages.

For the time being, when examining effects at a single age, we can consider the low-mass rotators in the Hyades and Praesepe as a single ensemble. The low-mass rotators deserve additional consideration in future work, but this will first require comprehensive binary surveys of late K and early M dwarfs to disentangle evolutionary effects from multiplicity effects in these clusters. Several authors have found tentative evidence that binaries rotate faster than single stars (e.g., Meibom et al. 2007; Douglas et al. 2016, 2017), which is one reason why we remove known binaries from our sample above.

The Hyades and Praesepe, however, have not been uniformly surveyed for binaries, particularly at the low-mass end. In our $K2$ analysis, we identify candidate binaries via blends and multiple periods detected in a single light curve. However, these candidates could be chance alignments or (when the two periods are very similar) a signal of latitudinal differential rotation.

NASA’s ongoing *Transiting Exoplanet Survey Satellite* mission (*TESS*; Ricker et al. 2015) will also provide an excellent opportunity for expanding the P_{rot} catalog for Hyades M dwarfs. Many Hyades M dwarfs lie on the outskirts of the cluster (with many more potentially found in unbound tidal tails; Röser et al. 2019), far enough from the ecliptic to be observed by *TESS*. Although there will certainly be issues with systematics given the standard 27.4 d observing cadence, we expect to measure P_{rot} for ≈ 200 Hyads in the Southern Hemisphere alone (*TESS* Program G011197). Many more Hyads, as well as members of another approximately

coeval Coma Ber cluster (Collier Cameron et al. 2009), will be observed by *TESS* in the Northern Hemisphere. Since one current challenge in comparing the Hyades and Praesepe is the much smaller Hyades P_{rot} catalog, future *TESS* measurements will be invaluable for differentiating the behavior of M dwarfs in these similarly aged clusters.

8. CONCLUSIONS

We analyze *K2* Campaign 13 light curves for 132 members of the Hyades open cluster. We measure P_{rot} for 116 (88%) of these stars, including 93 members with no prior P_{rot} measurements, bringing the total number of Hyads with known P_{rot} to 232. As in our last two papers (Douglas et al. 2016, 2017), we find that ground-based P_{rot} measurements are generally consistent with space-based measurements. The primary difference is that space-based observatories can observe a wide field of view nearly continuously while simultaneously reaching even faint members of nearby open clusters.

We then use *Gaia* DR2 data and literature binary information to define a clean sequence of single-star Hyads in color-magnitude space. We then apply this procedure to data for the Praesepe open cluster, which is generally thought to be coeval with the Hyades. As a result, we obtain two clean sequences of slowly rotating FGK stars in T_{eff} – P_{rot} space for both clusters.

There are far fewer known binaries among the M dwarfs in these two clusters. But our cuts also produce a nearly clean slow-rotator sequence for early M dwarfs, with only a few rapidly rotating members in this mass range in both clusters. These remaining rapid rotators highlight the need for additional binary surveys of M dwarfs in these clusters, especially Praesepe.

We use these single-star sequences to derive a reddening value of $A_V = 0.035 \pm 0.011$ mag for Praesepe, assuming that the Hyades experiences no reddening. This value is intermediate between the oft-assumed $A_V = 0.0$ and the $A_V = 0.084$ mag derived by Taylor (2006) for Praesepe. We then derive a polynomial fit to the slow rotator sequence in Praesepe, as a function of dereddened *Gaia* DR2 ($G_{BP} - G_{RP}$)₀ color. We use this fit as the basis for a new empirical model for gyrochronology, where we assume that stars begin on the Praesepe sequence at 670 Myr and their periods evolve as $P_{rot} \propto t^n$. By comparing the Praesepe sequence to the Sun, we derive a value of $n = 0.619$.

Finally, we compare the slow-rotator sequence in the Hyades to this model we have generated based on Praesepe. We find that, if we only consider the F and G stars, the Hyades is 57 Myr older than Praesepe. We also find,

however, that the difference between the Hyades and Praesepe sequences decreases towards lower-mass stars, so that the K and early M dwarfs in the two clusters are indistinguishable. This provides further evidence for stalling in the rotational evolution of these stars, and highlights the need for more detailed analysis of spin-down over time for stars of different masses.

S.T.D. acknowledges support provided by the NSF through grant AST-1701468. J.L.C. acknowledges support provided by the NSF through grant AST-1602662. M.A.A. acknowledges support provided by NASA through K2GO4 grant NNX17AF73G and by the NSF through grant AST-1255419. We also thank the anonymous referee for comments which improved the manuscript.

We thank R. Stefanik for sharing his Hyades binary detections with us. We also thank D. Latham for contributing to those observations and for providing valuable advice.

This research has made use of NASA’s Astrophysics Data System Bibliographic Services, the SIMBAD database (Wenger et al. 2000), operated at CDS, Strasbourg, France, and the VizieR database of astronomical catalogs (Ochsenbein et al. 2000).

This paper includes data collected by the *K2* mission. Funding for the *K2* mission was provided by the NASA Science Mission directorate.

This work has made use of data from the European Space Agency (ESA) mission *Gaia* (<https://www.cosmos.esa.int/gaia>), processed by the *Gaia* Data Processing and Analysis Consortium (DPAC, <https://www.cosmos.esa.int/web/gaia/dpac/consortium>). Funding for the DPAC has been provided by national institutions, in particular the institutions participating in the *Gaia* Multilateral Agreement.

This research has made use of the NASA/ IPAC Infrared Science Archive, which is operated by the Jet Propulsion Laboratory, California Institute of Technology, under contract with the National Aeronautics and Space Administration. The Two Micron All Sky Survey was a joint project of the University of Massachusetts and IPAC.

The Digitized Sky Survey was produced at the Space Telescope Science Institute under U.S. Government grant NAG W-2166. The images of these surveys are based on photographic data obtained using the Oschin Schmidt Telescope on Palomar Mountain and the UK Schmidt Telescope. The plates were processed into the present compressed digital form with the permission of these institutions.

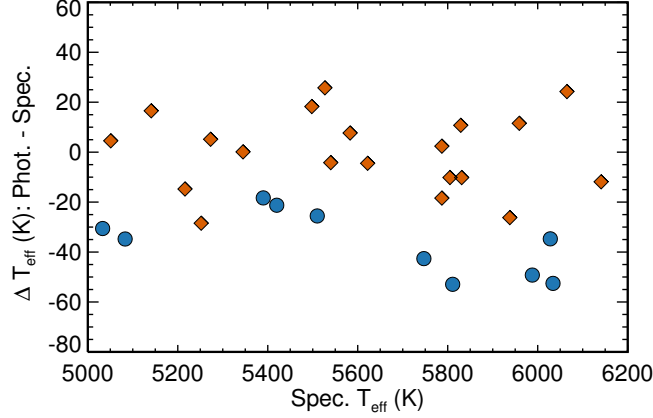


Figure 10. The difference between photometric ($T_{\text{eff,phot}}$) and spectroscopic effective temperatures ($T_{\text{eff,spec}}$) for 20 FGK members of the Hyades (orange diamonds) and nine of Praesepe (blue circles) are plotted against $T_{\text{eff,spec}}$. $T_{\text{eff,phot}}$ values are estimated based on the relationship between the *Gaia* DR2 color ($G_{\text{BP}} - G_{\text{RP}}$) and $T_{\text{eff,spec}}$ for the Hyads, which we assume appear to us un-reddened. We interpret stars with $T_{\text{eff,phot}} < T_{\text{eff,spec}}$ as reddened and extinguished by interstellar dust. Based on Praesepe’s median negative offset, we estimate $A_V = 0.035 \pm 0.01$ for that cluster.

APPENDIX

A. NON-ZERO REDDENING IN PRAESEPE

Praesepe suffers little interstellar reddening and extinction. Many studies—including our own prior work—assume zero reddening (e.g., Douglas et al. 2014; Angus et al. 2015; Douglas et al. 2017; Cummings et al. 2017) due to the cluster’s close proximity to Earth. Taylor (2006), however, found $E(B-V) = 0.027$ (or $A_V = 0.084$).

Interstellar reddening is often constrained with color–color diagram or CMD analyses. We take an alternative approach using spectroscopy. Co-author J. Brewer has observed members of the Hyades and Praesepe with Keck/HIRES for a separate project, and analyzed the spectra with Spectroscopy Made Easy (Valenti & Fischer 2005) following the Brewer et al. (2015) procedure (see also Brewer et al. 2016; Brewer & Fischer 2018). We match their target list with *Gaia* DR2 and filter out non-single star members according to their proximity to the empirical cluster main-sequence defined by the Gaia Collaboration et al. (2018a) membership list and their astrometry. We also only focus on those stars with $5000 < T_{\text{eff}} < 6200$ K, giving us 20 FGK stars in our Hyades sample and nine in our Praesepe sample.

We fit an empirical color–temperature relation to the Hyades sample, and define its reddening to be zero. Figure 10 compares the Praesepe stars with their Hyades analogs, and shows that the Praesepe stars have photometric temperatures that are systematically cooler than their spectroscopic temperatures. Spectroscopic and photometric temperatures for individual stars are given in Table 5. We then calculate the necessary reddening values for each star in the Hyades and Praesepe needed to align their photometric and spectroscopic temperatures. We find $A_V = 0.035 \pm 0.011$ (median and 1σ) for Praesepe. Our result splits the difference between the Taylor (2006) value and the oft-assumed zero reddening.

B. THE SUN’S GAIA DR2 COLOR

Since *Gaia* cannot observe the Sun’s disk-integrated light, we must instead estimate its *Gaia* color with analogous field stars. We select stars in the updated SPOCS catalog (Brewer et al. 2016) with spectroscopic properties most similar to the Sun’s, identifying 11 stars with T_{eff} within 100 K of 5777 K (the solar T_{eff} adopted by SPOCS), $\log g > 4.3$ dex, $[\text{Fe}/\text{H}]$ within 0.05 dex of solar, and $\log R'_{\text{HK}} < -4.8$ dex.

We then fit a cubic polynomial relating T_{eff} to color for these stars, finding that $T_{\text{eff}} = 5777$ K predicts a solar color $((G_{\text{BP}} - G_{\text{RP}}))_{\odot} = 0.817$ mag. This empirical value is in excellent agreement with that of Casagrande & Vandenberg (2018), who estimated the solar color from a variety of spectral templates to be $((G_{\text{BP}} - G_{\text{RP}}))_{\odot} = 0.82$ mag.

The SPOCS star that we decided was most similar to the Sun is HD 103828 (Gaia DR2 845471463339146496). It has the following spectroscopic properties in Brewer et al. (2016): $T_{\text{eff}} = 5771$ K, $\log g = 4.39$ dex, metallicity $[\text{M}/\text{H}] =$

Table 5. Praesepe and Hyades members used to derive the differential reddening between the two clusters

Cluster	DR2Name	SpecTeff	$(G_{\text{BP}} - G_{\text{RP}})$	PhotTeff
Praesepe	662925629454594944	5988	0.785	5939.1342
Praesepe	664683130070043136	5811	0.841	5758.5828
Praesepe	662841379375655936	5420	0.959	5398.3781
Praesepe	659539236719824768	6028	0.768	5993.4307
Praesepe	659766114072052608	5083	1.111	5049.5066
Praesepe	659343626729512832	6034	0.771	5981.6420
Praesepe	664600804138934400	5390	0.969	5371.2551
Praesepe	664366779961036288	5510	0.930	5484.3133
Praesepe	659768038217395968	5747	0.858	5704.8021
Hyades	47019347749289216	5141	1.055	5157.4270
Hyades	52548241968465408	5345	0.979	5344.6499
Hyades	49005581144118784	5527	0.907	5552.8148
Hyades	47345009348203392	5622	0.886	5617.7784
Hyades	3312644885984344704	5540	0.912	5535.8121
Hyades	3312575685471393664	5938	0.793	5912.2090
Hyades	3309956850635519488	5216	1.035	5200.8830
Hyades	3309006602007842048	5787	0.831	5789.9270
Hyades	3411887595780736128	5252	1.026	5223.1113
Hyades	3406823245223942528	5273	1.004	5277.6612
Hyades	3405113740864365440	6065	0.738	6088.7928
Hyades	3407121831350730112	5583	0.894	5590.8317
Hyades	100254161710940928	5787	0.838	5769.1275
Hyades	8479094371605632	5051	1.107	5056.6689
Hyades	10608573516849536	5959	0.775	5970.7933
Hyades	149005270337201792	5831	0.821	5821.3471
Hyades	145325548516513280	5498	0.919	5516.2169
Hyades	3313689422030650496	5805	0.830	5795.3730
Hyades	3306922958753764992	6141	0.725	6128.2910
Hyades	3309170875916905856	5829	0.816	5840.2860

-0.02 dex, and $v \sin i = 1.2$ km s $^{-1}$. The average chromospheric emission is $\log R'_{\text{HK}} = -4.846$ (Isaacson & Fischer 2010), corresponding to a chromospheric age of 3.89 Gyr (Mamajek & Hillenbrand 2008). The [Y/Mg] abundance ratio implies an age of 6.4 Gyr (Spina et al. 2018). The DR2 color for this star is $((G_{\text{BP}} - G_{\text{RP}})) = 0.8162$ mag.

HD 222582 (Gaia DR2 2440578577126302336) is also quite similar to the Sun, with $T_{\text{eff}} = 5789$ K, $\log g = 4.38$ dex, $[\text{M}/\text{H}] = +0.01$ dex, and $v \sin i = 0.5$ km s $^{-1}$. The average chromospheric emission is $\log R'_{\text{HK}} = -4.922$ (Isaacson & Fischer 2010), corresponding to a chromospheric age of 5.2 Gyr (Mamajek & Hillenbrand 2008). The [Y/Mg] abundance ratio implies an age of 6.7 Gyr (Spina et al. 2018). The DR2 color for this star is $((G_{\text{BP}} - G_{\text{RP}})) = 0.8201$ mag.

The solar twin 18 Sco (HD 146233) has $T_{\text{eff}} = 5785$ K, $\log g = 4.41$ dex, $[\text{M}/\text{H}] = +0.04$ dex, $v \sin i = 1.5$ km s $^{-1}$, and $\log R'_{\text{HK}} = -4.933$ dex. It has DR2 color of 0.8081 mag, which is only 0.009 less than our adopted solar value.

C. GYROCHRONOLOGICAL AGES FOR INDIVIDUAL HYADES AND PRAESEPE STARS

Facilities: Kepler (K2)

Software: Astropy (Astropy Collaboration et al. 2013), Astroquery (Ginsburg et al. 2013), AstroML (VanderPlas et al. 2012; Ivezić et al. 2013), pywcsgrid2 (J. Lee),⁸ K2fov (Mullally et al. 2016)

REFERENCES

⁸ <https://github.com/leejjoon/pywcsgrid2>

Table 6. gyrochronological ages for cluster members

Cluster	DR2Name	EPIC	PhotTeff	Gyro Age
			(K)	(Myr)
Praesepe	661311752544248960	211971871	6289.11	634.714
Praesepe	66140112222244032	211980688	6014.5	706.947
Praesepe	661317250102375040	211974702	5495.69	620.683
Praesepe	661319483485360000	211979334	5832.3	639.12
Praesepe	661243273585808000	211949471	6042.46	739.369
Praesepe	661277461525419008	211947686	6054.86	657.916
Praesepe	661319547906689024	211980170	5204.55	644.999
Praesepe	661292511090872960	211956059	5659.8	666.701
Praesepe	661244270018200064	211952381	6333.42	934.809
Praesepe	661207024061874944	211926132	6098.54	670.077
Praesepe	664387808120781056	211995288	5678.54	602.454
Praesepe	664302424170984960	211971690	5684.81	740.524
Praesepe	661424074527577984	211998346	6117.38	721.674
Praesepe	659687498990893056	211910082	6026.83	672.431
Praesepe	664403991557399040	212018902	5584.4	687.17
Praesepe	659758967246507008	211934056	5391.99	623.933
Praesepe	664311392062658048	211983461	5740.2	653.706
Praesepe	664437286143574016	212012299	5078.86	677.003
Praesepe	661028662658248960	211925093	5469.56	663.474
Praesepe	661401225301656064	211982334	5449.49	734.842
Praesepe	661300993647980032	211967293	5181.36	656.705
Praesepe	664334035130360064	211983499	5037.35	611.489
Praesepe	660998975844267008	211911846	5554.36	693.469
Praesepe	664283079638402944	211959522	5405.09	630.049
Praesepe	659755630055476992	211925552	5075.03	639.126
Praesepe	664366779961036032	211992034	5494.28	695.63
Praesepe	661029384212747008	211929531	5208.1	734.605
Praesepe	664497209527232000	212019439	5058.83	620.356
Praesepe	659665096441437056	211895099	6016.77	890.296
Praesepe	665129291274350976	212075775	5492.58	674.2
Praesepe	661422837576999040	211994672	5228.23	704.099
Praesepe	661295324291154944	211959779	5309.35	532.333
Praesepe	661029727808614016	211927269	5230.53	649.736
Praesepe	659766114072052992	211931128	5026.11	687.499
Praesepe	661338858079664000	211967873	5035.94	680.82
Praesepe	660944717521395968	211900700	5105.37	827.693
Praesepe	661222279785744000	211936827	5167.1	512.48
Praesepe	665004702861616000	212080687	6164.63	667.983
Praesepe	664283522018091008	211958260	5060.73	658.382
Praesepe	659343626729512960	211842439	5971.6	698.018
Praesepe	661325908755276032	211953567	5470.68	669.828
Praesepe	661239390935361024	211948267	5023.77	660.063
Praesepe	662925629454594944	211955365	5929.1	622.924
Hyades	3313662896312488192		5896.61	756.949
Hyades	3314109916508904064		5917.49	708.125
Hyades	45367056650753280		5954.75	767.84
Hyades	3312575685471393664		5856.73	885.692
Hyades	14900527037201792	211037886	5769.26	726.991
Hyades	3313689422030650496		5744.58	752.555
Hyades	3309006602007842048		5739.42	650.624
Hyades	47345009348203392		5578.14	710.055
Hyades	48061409893621248		5513.63	1029.32
Hyades	49005581144118784		5517.61	745.346
Hyades	3312644885984344704		5501.74	793.994
Hyades	145325548516513280	210899260	5483.42	703.103
Hyades	68001499939741440		5213.03	676.919
Hyades	3314213025787054592	210666330	5286.06	851.798
Hyades	43538293935879680		5090.25	700.693

- Agüeros, M. A., Covey, K. R., Lemonias, J. J., et al. 2011, *ApJ*, 740, 110
- Agüeros, M. A., Bowsher, E. C., Bochanski, J. J., et al. 2018, *ApJ*, 862, 33
- Aigrain, S., Parviainen, H., & Pope, B. 2016, *MNRAS*, stw706
- Alam, S., Albareti, F. D., Allende Prieto, C., et al. 2015, *ApJS*, 219, 12
- Andrae, R., Fouesneau, M., Creevey, O., et al. 2018, ArXiv e-prints, arXiv:1804.09374
- Angus, R., Aigrain, S., Foreman-Mackey, D., & McQuillan, A. 2015, *Monthly Notices of the Royal Astronomical Society*, 450, 1787
- Astropy Collaboration, Robitaille, T. P., Tollerud, E. J., et al. 2013, *A&A*, 558, A33
- Barnes, S. A. 2003, *ApJ*, 586, 464
- . 2007, *apj*, 669, 1167
- . 2010, *ApJ*, 722, 222
- Bopp, B. W., & Evans, D. S. 1973, *MNRAS*, 164, 343
- Boyajian, T. S., von Braun, K., van Belle, G., et al. 2012, *ApJ*, 757, 112
- Brandt, T. D., & Huang, C. X. 2015a, *ApJ*, 807, 58
- . 2015b, *ApJ*, 807, 24
- Brewer, J. M., & Fischer, D. A. 2018, *ApJS*, 237, 38
- Brewer, J. M., Fischer, D. A., Basu, S., Valenti, J. A., & Piskunov, N. 2015, *ApJ*, 805, 126
- Brewer, J. M., Fischer, D. A., Valenti, J. A., & Piskunov, N. 2016, *ApJS*, 225, 32
- Brown, T. M. 2014, *ApJ*, 789, 101
- Cargile, P. A., James, D. J., Pepper, J., et al. 2014, *ApJ*, 782, 29
- Casagrande, L., & VandenBerg, D. A. 2018, *MNRAS*, 479, L102
- Chaussidon, M. 2007, Formation of the Solar System: a Chronology Based on Meteorites, ed. M. Gargaud, H. Martin, & P. Claeys (Lectures in Astrobiology, 2007), 45
- Choi, J., Dotter, A., Conroy, C., et al. 2016, *ApJ*, 823, 102
- Collier Cameron, A., Davidson, V. A., Hebb, L., et al. 2009, *MNRAS*, 400, 451
- Cummings, J. D., Deliyannis, C. P., Maderak, R. M., & Steinhauer, A. 2017, *AJ*, 153, 128
- Cummings, J. D., Kalirai, J. S., Tremblay, P.-E., Ramirez-Ruiz, E., & Choi, J. 2018, ArXiv e-prints, arXiv:1809.01673
- Cutri, R. M., Skrutskie, M. F., van Dyk, S., et al. 2003, VizieR Online Data Catalog, 2246
- David, T. J., & Hillenbrand, L. A. 2015, *ApJ*, 804, 146
- Delorme, P., Collier Cameron, A., Hebb, L., et al. 2011, *MNRAS*, 413, 2218
- Donahue, R. A., Saar, S. H., & Baliunas, S. L. 1996, *ApJ*, 466, 384
- Douglas, S. T., Agüeros, M. A., Covey, K. R., et al. 2016, *ApJ*, 822, 47
- Douglas, S. T., Agüeros, M. A., Covey, K. R., & Kraus, A. 2017, *The Astrophysical Journal*, 842, 83
- Douglas, S. T., Agüeros, M. A., Covey, K. R., et al. 2014, *ApJ*, 795, 161
- Eker, Z. 1994, *ApJ*, 420, 373
- Fossati, L., Bagnulo, S., Landstreet, J., et al. 2008, *A&A*, 483, 891
- Gaia Collaboration, Babusiaux, C., van Leeuwen, F., et al. 2018a, *A&A*, 616, A10
- Gaia Collaboration, Brown, A. G. A., Vallenari, A., et al. 2018b, *A&A*, 616, A1
- Garraffo, C., Drake, J. J., Dotter, A., et al. 2018, *ApJ*, 862, 90
- Ginsburg, A., Robitaille, T., Parikh, M., et al. 2013, Astroquery v0.1, doi:10.6084/m9.figshare.805208.v2
- Goldman, B., Röser, S., Schilbach, E., et al. 2013, *Astronomy & Astrophysics*, 559, A43
- Gossage, S., Conroy, C., Dotter, A., et al. 2018, *ApJ*, 863, 67
- Gunn, J. E., Griffin, R. F., Griffin, R. E. M., & Zimmerman, B. A. 1988, *AJ*, 96, 198
- Hartman, J. D., Bakos, G. Á., Noyes, R. W., et al. 2011, *AJ*, 141, 166
- Hodgkin, S. T., Pinfield, D. J., Jameson, R. F., et al. 1999, *MNRAS*, 310, 87
- Isaacson, H., & Fischer, D. 2010, *ApJ*, 725, 875
- Ivezic, Ž., Connolly, A., VanderPlas, J., & Gray, A. 2013, Statistics, Data Mining, and Machine Learning in Astronomy
- Kopytova, T. G., Brandner, W., Tognelli, E., et al. 2016, *A&A*, 585, A7
- Kovács, G., Hartman, J. D., Bakos, G. Á., et al. 2014, *MNRAS*, 442, 2081
- Kraus, A. L., & Hillenbrand, L. A. 2007, *AJ*, 134, 2340
- Mamajek, E. E., & Hillenbrand, L. A. 2008, *ApJ*, 687, 1264
- Mann, A. W., Feiden, G. A., Gaidos, E., Boyajian, T., & von Braun, K. 2015, *ApJ*, 804, 64
- Mann, A. W., Gaidos, E., Vanderburg, A., et al. 2017, *AJ*, 153, 64
- Mason, B. D., Hartkopf, W. I., Holdenried, E. R., & Rafferty, T. J. 2001, *AJ*, 121, 3224
- Matt, S. P., Brun, A. S., Baraffe, I., Bouvier, J., & Chabrier, G. 2015, *ApJL*, 799, L23
- Meibom, S., Barnes, S. A., Platais, I., et al. 2015, *Nature*, 517, 589
- Meibom, S., & Mathieu, R. D. 2005, *ApJ*, 620, 970

- Meibom, S., Mathieu, R. D., & Stassun, K. G. 2007, ApJL, 665, L155
- Meibom, S., Mathieu, R. D., & Stassun, K. G. 2009, ApJ, 695, 679
- Meibom, S., Mathieu, R. D., Stassun, K. G., Liebesny, P., & Saar, S. H. 2011a, ApJ, 733, 115
- Meibom, S., Barnes, S. A., Latham, D. W., et al. 2011b, ApJ, 733, L9
- Mermilliod, J.-C., Mayor, M., & Udry, S. 2009, A&A, 498, 949
- Morzinski, K. M. 2011, PhD thesis, University of California, Santa Cruz
- Mullally, F., Barclay, T., & Barentsen, G. 2016, Astrophysics Source Code Library, ascl:1601.009
- Ochsenbein, F., Bauer, P., & Marcout, J. 2000, ApJS, 143, 23
- Patience, J., Ghez, A. M., Reid, I. N., Weinberger, A. J., & Matthews, K. 1998, The Astronomical Journal, 115, 1972
- Perryman, M. A. C., Brown, A. G. A., Lebreton, Y., et al. 1998, Astronomy and Astrophysics, 331, 81
- Pojmański, G. 2002, Acta Astronomica, 52, 397
- Press, W. H., & Rybicki, G. B. 1989, ApJ, 338, 277
- Prosser, C. F., Shetrone, M. D., Dasgupta, A., et al. 1995, PASP, 107, 211
- Quinn, S. N., White, R. J., Latham, D. W., et al. 2012, ApJL, 756, L33
- Rabus, M., Lachaume, R., Jordán, A., et al. 2019, MNRAS, arXiv:1901.08077
- Radick, R. R., Lockwood, G. W., Skiff, B. A., & Thompson, D. T. 1995, ApJ, 452, 332
- Radick, R. R., Thompson, D. T., Lockwood, G. W., Duncan, D. K., & Baggett, W. E. 1987, ApJ, 321, 459
- Rebull, L. M., Stauffer, J. R., Hillenbrand, L. A., et al. 2017, ApJ, 839, 92
- Reiners, A., & Mohanty, S. 2012, ApJ, 746, 43
- Ricker, G. R., Winn, J. N., Vanderspek, R., et al. 2015, Journal of Astronomical Telescopes, Instruments, and Systems, 1, 014003
- Röser, S., Schilbach, E., & Goldman, B. 2019, A&A, 621, L2
- Röser, S., Schilbach, E., Piskunov, A. E., Kharchenko, N. V., & Scholz, R.-D. 2011, Astronomy and Astrophysics, 531, A92
- Scholz, A., & Eislöffel, J. 2007, MNRAS, 381, 1638
- Scholz, A., Irwin, J., Bouvier, J., et al. 2011, MNRAS, 413, 2595
- Skrutskie, M. F., Cutri, R. M., Stiening, R., et al. 2006, AJ, 131, 1163
- Skumanich, A. 1972, The Astrophysical Journal, 171, 565
- Spina, L., Meléndez, J., Karakas, A. I., et al. 2018, MNRAS, 474, 2580
- Taylor, B. J. 2006, AJ, 132, 2453
- Valenti, J. A., & Fischer, D. A. 2005, ApJS, 159, 141
- van Saders, J. L., Ceillier, T., Metcalfe, T. S., et al. 2016, Nature, 529, 181
- van Saders, J. L., & Pinsonneault, M. H. 2013, ApJ, 776, 67
- VanderPlas, J., Connolly, A. J., Ivezić, Z., & Gray, A. 2012, eprint: arXiv:1411.5039, 47–54
- Wenger, M., Ochsenbein, F., Egret, D., et al. 2000, A&AS, 143, 9
- Zacharias, N., Finch, C., Girard, T., et al. 2010, AJ, 139, 2184
- Zahn, J.-P. 2008, in EAS Publications Series, Vol. 29, EAS Publications Series, 67–90, eprint: arXiv:0807.4870